Defect Identification in Composite Structures Using Enhanced Signal Analysis

Shen Hin Lim and Tomonari Furukawa
IALR, 150 Slayton Avenue, Danville, VA 24540
Department of Mechanical Engineering
Virginia Polytechnic Institute and State University

Final Report for FA23860814112

Background

The most commonly used NDI techniques for composite structures are based on the transmission and reflection of ultrasonic waves in composite structures. The patterns of such reflected and transmitted signals are used to detect anomalies in the structure indicating defects. Many such systems are commercially available and are widely used in manufacturing for production quality control and in maintenance of structures to detect defects due to operational factors. The calibration of such systems and the interpretation of the results to detect and characterize defects rely on skilled and experienced operators. The thorough inspection and evaluation of large structures is labor intensive and involves long elapse times.

Aims and Objectives

Aims

The aim of this project is to develop a new approach and its theoretical and experimental framework, where this approach is able to automatically and rapidly quantify invisible defects in a composite structure through enhanced analysis of data from ultrasonic non-destructive inspection methods.

Objectives

The objectives of this project are to develop rapid automated techniques to:

- Interrogate output from ultrasonic NDI equipment to identify the presence of defects.
- Identify the type of defect, in particular delamination, disbanding, foreign body inclusions and porosity.
- Characterize the damage with respect to its location and size.

The completed research tasks to achieve the aims and objectives of this project are classified into two categories:

- Theoretical framework: Stochastic defect identification under sensor uncertainties
- Rapid field inspection by optimally guiding and controlling sensors

Research Tasks

Report Documentation Page

Form Approved
OMB No. 0704-0188

1. REPORT DATE	2. REPORT TYPE	3. DATES COVERED
07 JAN 2011	**FInal**	**22-12-2008 to 22-12-2011**

4. TITLE AND SUBTITLE
Defect Identification In Composite Structures Using Enhanced Signal Analysis

5a. CONTRACT NUMBER
FA23860814112

5b. GRANT NUMBER

5c. PROGRAM ELEMENT NUMBER

6. AUTHOR(S)
Tomonari Furukawa

5d. PROJECT NUMBER

5e. TASK NUMBER

5f. WORK UNIT NUMBER

7. PERFORMING ORGANIZATION NAME(S) AND ADDRESS(ES)
Virginia Polytechnic Institute and State University,Dept. of Mechanical Engineering,Blacksburg, ,VA,VA,24061-0238

8. PERFORMING ORGANIZATION REPORT NUMBER
N/A

9. SPONSORING/MONITORING AGENCY NAME(S) AND ADDRESS(ES)
AOARD, UNIT 45002, APO, AP, 96337-5002

10. SPONSOR/MONITOR'S ACRONYM(S)
AOARD

11. SPONSOR/MONITOR'S REPORT NUMBER(S)
AOARD-084112

12. DISTRIBUTION/AVAILABILITY STATEMENT
Approved for public release; distribution unlimited

13. SUPPLEMENTARY NOTES

14. ABSTRACT

This project developed a new approach with theoretical and experimental framework to automatically and rapidly quantify invisible defects in a composite structure through enhanced analysis of data from ultrasonic non-destructive inspection methods. The objectives of this project were to develop rapid automated techniques to: Interrogate output from ultrasonic NDI equipment to identify the presence of defects, Identify the type of defect, in particular delamination, disbanding, foreign body inclusions and porosity and Characterize the damage with respect to its location and size. Theoretical framework consisted of stochastic defect identification under sensor uncertainties and rapid field inspection by optimally guiding and controlling sensors. The system constructed from this project has the following capabilities: Automated techniques to characterize defects; Technique that stochastically estimates the states of defects; Technique that allows active sensing; and Technique that enhances current signal analysis.

15. SUBJECT TERMS
Non-destructive Evaluation, mechanics

16. SECURITY CLASSIFICATION OF:			17. LIMITATION OF ABSTRACT	18. NUMBER OF PAGES	19a. NAME OF RESPONSIBLE PERSON
a. REPORT	b. ABSTRACT	c. THIS PAGE			
unclassified	**unclassified**	**unclassified**	**Same as Report (SAR)**	**27**	

Theoretical framework: Stochastic defect identification under sensor uncertainties

Theoretical formulation (Both Bayesian and KF)

A sensor for NDE consisting of transmitter(s) and receiver(s), *s* is not fixed and thus has the motion model

$$\mathbf{x}_k^s = \mathbf{f}^s\left(\mathbf{x}_{k-1}^s, \mathbf{u}_k^s, \mathbf{w}_k^s\right)$$

where $\mathbf{x}_k^s \in \chi^s$ is the state, $\mathbf{u}_k^s$ is the control input and $\mathbf{w}_k^s$ is the "system noise" of the sensor at time step *k*. The motion model of *i*th defect d_i, is given by

$$\mathbf{x}_k^{d_i} = \mathbf{x}_{k-1}^{d_i}$$

as the defect is stationary, and $\mathbf{x}_k^{d_i} \in \chi^d$ is the state of *i*th defect at time step *k*. The defect is detected and localized by the observations from the NDE sensor with respect to the NDE sensor frame. To develop its model, let the field of view, or the observable region, of the sensor as

$${}^sX_O^d \equiv \left\{\mathbf{x}_k^{d_i} \mid 0 < P_D\left(\mathbf{x}_k^{d_i} \mid \mathbf{x}_k^s\right)\right\}$$

which is influenced by a probability of detecting a single defect d_i $P_D\left(\mathbf{x}_k^{d_i} \mid \mathbf{x}_k^s\right)$. Then, the observation model of the NDE sensor is probabilistically expressed as

$${}^s\mathbf{z}_k^{d_i} = \begin{cases} {}^s\mathbf{h}^d\left(\mathbf{x}_k^s, \mathbf{x}_k^{d_i}, {}^s\mathbf{v}_k^{d_i}\right) & \exists \mathbf{x}_k^{d_i} \in {}^sX_O^d \\ \varnothing & \nexists \mathbf{x}_k^{d_i} \in {}^sX_O^d \end{cases}$$

where ${}^s\mathbf{z}_k^{d_i}$ and ${}^s\mathbf{v}_k^{d_i}$ are an observation and its observation noise, and $\varnothing$ represents an ``empty element", indicating that the observation contains no information on the defect or the defect is unobservable since it is not within the observable region. In order to detect and localize defects with respect to a structure frame, the proposed approach further assumes the implementation of either an on-board device or a global measurement device for observation on the NDE sensor location with respect to the structure frame. The model of this observation can be described as

$$\mathbf{z}_k^s = \mathbf{h}^s\left(\mathbf{x}_k^s, \mathbf{v}_k^s\right)$$

with its observation noise $\mathbf{v}_k^s$. Suppose that *n* defects have been detected by the NDE sensor at time step *k*. Observations available from and on the NDE sensor, which have been synchronously measured, are a sequence of readings on the NDE sensor location, $\tilde{\mathbf{z}}_{1:k}^s = \left\{\tilde{\mathbf{z}}_1^s, \ldots, \tilde{\mathbf{z}}_k^s\right\}$ and a sequence of readings on n defects from the NDE sensor, $\tilde{\mathbf{z}}_{1:k}^{d_i} = \left\{\tilde{\mathbf{z}}_1^{d_i}, \ldots, \tilde{\mathbf{z}}_k^{d_i}\right\}$, $\forall i \in \{1, \ldots, n\}$ though some observations could be empty. The notation $\left(\tilde{\cdot}\right)$ indicates an instance of $\left(\cdot\right)$. Under the condition, the defect identification can be defined as identifying the locations of the *n* defects given by these observations, $\mathbf{x}_k^{d_i}$, $\forall i \in \{1, \ldots, n\}$. Since the defect locations identified are to be described with some confidence, it is more precise to say

that the objective is to best update the belief $p\left(\mathbf{x}_k^{d_i}\right)$ under the influence of the NDE sensor belief $p\left(\mathbf{x}_k^{s}\right)$, where $p(\cdot)$ represents a probability density function.

Sensor and Observation Models

The proposed stochastic defect identification technique starts with the approximation of motion and observation models by Gaussian distributions as the Gaussian assumption is valid if the frequency of update is high and the update is performed only based on positive observations. In defect identification, the Gaussian assumption approximates and completes the motion models of the NDE sensor and the defects as

$$\mathbf{x}_k^s = \mathbf{f}^s\left(\mathbf{x}_{k-1}^s, \mathbf{u}_k^s\right) + \mathbf{w}_k^s$$
$$\mathbf{x}_k^{d_i} = \mathbf{x}_{k-1}^{d_i}, \forall i \in \{1,\ldots,n\}$$

with the system noise $\mathbf{w}_k^s \sim N\left(\mathbf{0}, \boldsymbol{\Sigma}_k^{\mathrm{w}^s}\right)$. The defect motion model is deterministic unless it propagates in time. Meanwhile, the observation models of the observations on and from the NDE sensor are both probabilistically given by

$$\mathbf{z}_k^s = \mathbf{x}_k^s + \mathbf{v}_k^s$$
$${}^s\mathbf{z}_k^{d_i} = -\mathbf{x}_k^s + \mathbf{x}_k^{d_i} + {}^s\mathbf{v}_k^{d_i}, \forall i \in \{1,\ldots,n\}$$

where $\mathbf{v}_k^s \sim N\left(\mathbf{0}, \boldsymbol{\Sigma}_k^{\mathrm{v}^s}\right)$ and ${}^s\mathbf{v}_k^{d_i} \sim N\left(\mathbf{0}, \boldsymbol{\Sigma}_k^{{}^s\mathrm{v}^{d_i}}\right)$. The observations are directly on the state of the NDE sensor and the state of the defect relative to the NDE sensor. The observation models are single-conditioned since the Gaussian assumption does not allow the observable region to be defined.

Sensor and Defect Identification

Having the motion and the observation models defined with the Gaussian assumption, the proposed technique updates the mean and the covariance of the NDE sensor and defects beliefs rather than their entire belief distributions using the EKF. The formulations of the EKF yield the mean of both the beliefs predicted from the mean of their respective previous beliefs as

$$\bar{\mathbf{x}}_{k|k-1}^s = \mathbf{f}^s\left(\bar{\mathbf{x}}_{k-1|k-1}^s, \tilde{\mathbf{u}}_k^s\right)$$
$$\mathbf{x}_{k|k-1}^{d_i} = \mathbf{x}_{k-1|k-1}^{d_i}$$

where $\mathbf{x}_{k|k-1}^{(\cdot)}$ represents the belief of $(\cdot)$ at time step *k* given observations up to *k*-1. The notation $\bar{(\cdot)}$ indicates a mean of belief. Since the NDE sensor and the defects have no correlation in motion, the prediction of covariance can also be independently treated although thorough matrix analysis is necessary. Let the bundled mean and the covariance of the NDE sensor and defects as $\bar{\mathbf{x}}_{k|k} \equiv \left[\bar{\mathbf{x}}_{k|k}^s, \bar{\mathbf{x}}_{k|k}^d\right]^\top = \left[\bar{\mathbf{x}}_{k|k}^s, \bar{\mathbf{x}}_{k|k}^{d_1}, \ldots, \bar{\mathbf{x}}_{k|k}^{d_n}\right]^\top$ and

$$\boldsymbol{\Sigma}^{\mathbf{x}}_{k|k} \equiv \boldsymbol{\Sigma}_{k|k} = \begin{bmatrix} \boldsymbol{\Sigma}^{ss}_{k|k} & \boldsymbol{\Sigma}^{sd}_{k|k} \\ \boldsymbol{\Sigma}^{ds}_{k|k} & \boldsymbol{\Sigma}^{dd}_{k|k} \end{bmatrix} = \begin{bmatrix} \boldsymbol{\Sigma}^{ss}_{k|k} & \boldsymbol{\Sigma}^{sd_1}_{k|k} & \cdots & \boldsymbol{\Sigma}^{sd_n}_{k|k} \\ \boldsymbol{\Sigma}^{d_1 s}_{k|k} & \boldsymbol{\Sigma}^{d_1 d_1}_{k|k} & \cdots & \boldsymbol{\Sigma}^{d_1 d_n}_{k|k} \\ \vdots & \vdots & \ddots & \vdots \\ \boldsymbol{\Sigma}^{d_n s}_{k|k} & \boldsymbol{\Sigma}^{d_n d_1}_{k|k} & \cdots & \boldsymbol{\Sigma}^{d_n d_n}_{k|k} \end{bmatrix}$$

and the observation as $\mathbf{z}_k \equiv \left[\mathbf{z}^s_k, {}^s\mathbf{z}^{d_1}_k, \ldots, {}^s\mathbf{z}^{d_n}_k\right]^\top$. The covariance prediction is collectively given by

$$\boldsymbol{\Sigma}^{\mathbf{x}}_{k|k-1} = \mathbf{A}_{k-1} \boldsymbol{\Sigma}^{\mathbf{x}}_{k-1|k-1} \mathbf{A}_{k-1}{}^\top + \boldsymbol{\Sigma}^{\mathbf{w}}_k$$

or, by knowing

$$\mathbf{A}_{k-1} = \begin{bmatrix} \mathbf{A}^{ss}_{k-1} & \mathbf{A}^{sd}_{k-1} \\ \mathbf{A}^{ds}_{k-1} & \mathbf{A}^{dd}_{k-1} \end{bmatrix}$$

with each element as

$$\begin{aligned} \mathbf{A}^{ss}_{k-1} &= \nabla_{\mathbf{x}^s_{k-1|k-1}} \mathbf{f}^s \left(\overline{\mathbf{x}}^s_{k-1|k-1}, \tilde{\mathbf{u}}^s_k \right) \\ \mathbf{A}^{sd}_{k-1} &= \mathbf{0} \\ \mathbf{A}^{ds}_{k-1} &= \mathbf{0} \\ \mathbf{A}^{dd}_{k-1} &= \mathbf{I}^{n,n} \end{aligned}$$

and

$$\boldsymbol{\Sigma}^{\mathbf{w}}_k = \begin{bmatrix} \boldsymbol{\Sigma}^{\mathbf{w}^s}_k & \mathbf{0} \\ \mathbf{0} & \mathbf{0} \end{bmatrix}$$

It is given in matrix-vector form as

$$\begin{aligned} &\begin{bmatrix} \boldsymbol{\Sigma}^{ss}_{k|k-1} & \boldsymbol{\Sigma}^{sd}_{k|k-1} \\ \boldsymbol{\Sigma}^{ds}_{k|k-1} & \boldsymbol{\Sigma}^{dd}_{k|k-1} \end{bmatrix} \\ &= \begin{bmatrix} \mathbf{A}^{ss}_{k-1} & \mathbf{0} \\ \mathbf{0} & \mathbf{I}^{n,n} \end{bmatrix} \begin{bmatrix} \boldsymbol{\Sigma}^{ss}_{k-1|k-1} & \boldsymbol{\Sigma}^{sd}_{k-1|k-1} \\ \boldsymbol{\Sigma}^{ds}_{k-1|k-1} & \boldsymbol{\Sigma}^{dd}_{k-1|k-1} \end{bmatrix} \begin{bmatrix} \mathbf{A}^{ss}_{k-1}{}^\top & \mathbf{0} \\ \mathbf{0} & \mathbf{I}^{n,n} \end{bmatrix} + \begin{bmatrix} \boldsymbol{\Sigma}^{\mathbf{w}^s}_k & \mathbf{0} \\ \mathbf{0} & \mathbf{0} \end{bmatrix} \\ &= \begin{bmatrix} \mathbf{A}^{ss}_{k-1} \boldsymbol{\Sigma}^{ss}_{k-1|k-1} \mathbf{A}^{ss}_{k-1}{}^\top & \mathbf{A}^{ss}_{k-1} \boldsymbol{\Sigma}^{sd}_{k-1|k-1} \\ \boldsymbol{\Sigma}^{ds}_{k-1|k-1} \mathbf{A}^{ss}_{k-1}{}^\top & \boldsymbol{\Sigma}^{dd}_{k-1|k-1} \end{bmatrix} + \begin{bmatrix} \boldsymbol{\Sigma}^{\mathbf{w}^s}_k & \mathbf{0} \\ \mathbf{0} & \mathbf{0} \end{bmatrix} \end{aligned}$$

or individually

$$\begin{aligned}
\boldsymbol{\Sigma}^{ss}_{k|k-1} &= \mathbf{A}^{ss}_{k-1}\boldsymbol{\Sigma}^{ss}_{k-1|k-1}\mathbf{A}^{ss\ \top}_{k-1} + \boldsymbol{\Sigma}^{\mathbf{w}^s}_{k} \\
\boldsymbol{\Sigma}^{sd}_{k|k-1} &= \mathbf{A}^{ss}_{k-1}\boldsymbol{\Sigma}^{sd}_{k-1|k-1} \\
\boldsymbol{\Sigma}^{ds}_{k|k-1} &= \boldsymbol{\Sigma}^{ds}_{k-1|k-1}\mathbf{A}^{ss\ \top}_{k-1} \\
\boldsymbol{\Sigma}^{dd}_{k|k-1} &= \boldsymbol{\Sigma}^{dd}_{k-1|k-1}
\end{aligned}$$

where $\mathbf{I}^{n,n}$ is an identity matrix of both row and column sizes with n set of state variables of a NDE sensor or a defect. Note that, to avoid complexity, the number of state variables of a NDE sensor and that of a defect are assumed to be identical in this paper. The correction of mean is given by

$$\overline{\mathbf{x}}_{k|k} = \overline{\mathbf{x}}_{k|k-1} + \mathbf{K}_k\left(\tilde{\mathbf{z}}_k - \mathbf{C}_k\overline{\mathbf{x}}_{k|k-1}\right)$$

or, with the elements of vectors and matrices,

$$\begin{bmatrix}\overline{\mathbf{x}}^{s}_{k|k}\\ \overline{\mathbf{x}}^{d}_{k|k}\end{bmatrix} = \begin{bmatrix}\overline{\mathbf{x}}^{s}_{k|k-1}\\ \overline{\mathbf{x}}^{d}_{k|k-1}\end{bmatrix} + \begin{bmatrix}\mathbf{K}^{ss}_{k} & \mathbf{K}^{sd}_{k}\\ \mathbf{K}^{ds}_{k} & \mathbf{K}^{dd}_{k}\end{bmatrix}\left(\begin{bmatrix}\tilde{\mathbf{z}}^{s}_{k}\\ {}^{s}\tilde{\mathbf{z}}^{d}_{k}\end{bmatrix} - \begin{bmatrix}\mathbf{I}^{1,1} & \mathbf{0}\\ -\mathbf{I}^{n,1} & \mathbf{I}^{n,n}\end{bmatrix}\begin{bmatrix}\overline{\mathbf{x}}^{s}_{k|k-1}\\ \overline{\mathbf{x}}^{d}_{k|k-1}\end{bmatrix}\right)$$

The matrix-vector representation results in the individual correction of a sensor and defects as:

$$\begin{aligned}
\overline{\mathbf{x}}^{s}_{k|k} &= \overline{\mathbf{x}}^{s}_{k|k-1} + \mathbf{K}^{ss}_{k}\left(\tilde{\mathbf{z}}^{s}_{k} - \overline{\mathbf{x}}^{s}_{k|k-1}\right) + \sum_{j=1}^{n}\mathbf{K}^{sd_j}_{k}\left({}^{s}\tilde{\mathbf{z}}^{d_j}_{k} + \overline{\mathbf{x}}^{s}_{k|k-1} - \overline{\mathbf{x}}^{d_j}_{k|k-1}\right) \\
\overline{\mathbf{x}}^{d}_{k|k} &= \overline{\mathbf{x}}^{d}_{k|k-1} + \mathbf{K}^{d1s}_{k}\left(\tilde{\mathbf{z}}^{s}_{k} - \overline{\mathbf{x}}^{s}_{k|k-1}\right) + \sum_{j=1}^{n}\mathbf{K}^{d_i d_j}_{k}\left({}^{s}\tilde{\mathbf{z}}^{d_j}_{k} + \overline{\mathbf{x}}^{s}_{k|k-1} - \overline{\mathbf{x}}^{d_j}_{k|k-1}\right)
\end{aligned}$$

The correction of covariance, on the other hand, is given by

$$\boldsymbol{\Sigma}_{k|k} = \left(\mathbf{I} - \mathbf{K}_k\mathbf{C}_k\right)\boldsymbol{\Sigma}_{k|k-1}$$

which, in matrix-vector form, can be written as

$$\begin{aligned}
&\begin{bmatrix}\boldsymbol{\Sigma}^{ss}_{k|k} & \boldsymbol{\Sigma}^{sd}_{k|k}\\ \boldsymbol{\Sigma}^{ds}_{k|k} & \boldsymbol{\Sigma}^{dd}_{k|k}\end{bmatrix} \\
&= \left(\begin{bmatrix}\mathbf{I}^{1,1} & \mathbf{0}\\ \mathbf{0} & \mathbf{I}^{n,n}\end{bmatrix} - \begin{bmatrix}\mathbf{K}^{ss}_{k} & \mathbf{K}^{sd}_{k}\\ \mathbf{K}^{ds}_{k} & \mathbf{K}^{dd}_{k}\end{bmatrix}\begin{bmatrix}\mathbf{I}^{1,1} & \mathbf{0}\\ -\mathbf{I}^{n,1} & \mathbf{I}^{n,n}\end{bmatrix}\right)\begin{bmatrix}\boldsymbol{\Sigma}^{ss}_{k|k-1} & \boldsymbol{\Sigma}^{sd}_{k|k-1}\\ \boldsymbol{\Sigma}^{ds}_{k|k-1} & \boldsymbol{\Sigma}^{dd}_{k|k-1}\end{bmatrix} \\
&= \begin{bmatrix}\mathbf{I}^{1,1} - \mathbf{K}^{ss}_{k} + \sum_{l=1}^{n}\mathbf{K}^{sd_l}_{k} & -\mathbf{K}^{sd}_{k}\\ -\mathbf{K}^{ds}_{k} + \left[\sum_{l=1}^{n}\mathbf{K}^{d_i d_l}_{k}\right]_{i=1,\ldots,n,\,j=1} & \mathbf{I}^{n,n} - \mathbf{K}^{dd}_{k}\end{bmatrix}\begin{bmatrix}\boldsymbol{\Sigma}^{ss}_{k|k-1} & \boldsymbol{\Sigma}^{sd}_{k|k-1}\\ \boldsymbol{\Sigma}^{ds}_{k|k-1} & \boldsymbol{\Sigma}^{dd}_{k|k-1}\end{bmatrix}
\end{aligned}$$

Thus, this derives each set of elements of the covariance as

$$\begin{aligned}
\boldsymbol{\Sigma}_{k|k}^{ss} &= \mathbf{P}_k^{11}\boldsymbol{\Sigma}_{k|k-1}^{ss} + \mathbf{P}_k^{12}\boldsymbol{\Sigma}_{k|k-1}^{ds} \\
\boldsymbol{\Sigma}_{k|k}^{ds} &= \mathbf{P}_k^{21}\boldsymbol{\Sigma}_{k|k-1}^{ss} + \mathbf{P}_k^{22}\boldsymbol{\Sigma}_{k|k-1}^{ds} \\
\boldsymbol{\Sigma}_{k|k}^{sd} &= \mathbf{P}_k^{11}\boldsymbol{\Sigma}_{k|k-1}^{sd} + \mathbf{P}_k^{12}\boldsymbol{\Sigma}_{k|k-1}^{dd} \\
\boldsymbol{\Sigma}_{k|k}^{dd} &= \mathbf{P}_k^{21}\boldsymbol{\Sigma}_{k|k-1}^{sd} + \mathbf{P}_k^{22}\boldsymbol{\Sigma}_{k|k-1}^{dd}
\end{aligned}$$

where

$$\begin{aligned}
\mathbf{P}_k^{11} &= \mathbf{I}^{1,1} - \mathbf{K}_k^{ss} + \sum_{l=1}^{n}\mathbf{K}_k^{sd_l} \\
\mathbf{P}_k^{12} &= -\mathbf{K}_k^{sd} \\
\mathbf{P}_k^{21} &= -\mathbf{K}_k^{ds} + \left[\sum_{l=1}^{n}\mathbf{K}_k^{d_i d_l}\right]_{i=1,\ldots,n,\, j=1} \\
\mathbf{P}_k^{22} &= \mathbf{I}^{n,n} - \mathbf{K}_k^{dd}
\end{aligned}$$

The Kalman gain that minimizes the trace of variances and enables optimal estimation is given by

$$\mathbf{K}_k = \boldsymbol{\Sigma}_{k|k-1}\mathbf{C}_k{}^{\top}\mathbf{S}_k{}^{-1} = \boldsymbol{\Sigma}_{k|k-1}\mathbf{C}_k{}^{\top}\left\{\mathbf{C}_k\boldsymbol{\Sigma}_{k|k-1}\mathbf{C}_k{}^{\top} + \boldsymbol{\Sigma}_k^{\mathbf{v}}\right\}^{-1}$$

which, in matrix-vector form, is

$$\begin{aligned}
\begin{bmatrix} \mathbf{K}_k^{ss} & \mathbf{K}_k^{sd} \\ \mathbf{K}_k^{ds} & \mathbf{K}_k^{dd} \end{bmatrix} &= \begin{bmatrix} \boldsymbol{\Sigma}_{k|k-1}^{ss} & \boldsymbol{\Sigma}_{k|k-1}^{sd} \\ \boldsymbol{\Sigma}_{k|k-1}^{ds} & \boldsymbol{\Sigma}_{k|k-1}^{dd} \end{bmatrix}\begin{bmatrix} \mathbf{I}^{1,1} & -\mathbf{I}^{1,n} \\ \mathbf{0} & \mathbf{I}^{n,n} \end{bmatrix}\begin{bmatrix} \mathbf{S}_k^{ss} & \mathbf{S}_k^{sd} \\ \mathbf{S}_k^{ds} & \mathbf{S}_k^{dd} \end{bmatrix}^{-1} \\
&= \begin{bmatrix} \boldsymbol{\Sigma}_{k|k-1}^{ss} & \left[-\boldsymbol{\Sigma}_{k|k-1}^{ss} + \boldsymbol{\Sigma}_{k|k-1}^{sd\,j}\right]_{i=1,\, j=1,\ldots,n} \\ \boldsymbol{\Sigma}_{k|k-1}^{ds} & \left[-\boldsymbol{\Sigma}_{k|k-1}^{d_i s} + \boldsymbol{\Sigma}_{k|k-1}^{d_i d\,j}\right]_{i=1,\ldots,n,\, j=1,\ldots,n} \end{bmatrix}\begin{bmatrix} \mathbf{S}_k^{ss} & \mathbf{S}_k^{sd} \\ \mathbf{S}_k^{ds} & \mathbf{S}_k^{dd} \end{bmatrix}^{-1}
\end{aligned}$$

where the matrix $\mathbf{S}_k$ is given by

$$
\begin{aligned}
\begin{bmatrix} \mathbf{S}_k^{ss} & \mathbf{S}_k^{sd} \\ \mathbf{S}_k^{ds} & \mathbf{S}_k^{dd} \end{bmatrix} &= \begin{bmatrix} \mathbf{I}^{1,1} & \mathbf{0} \\ -\mathbf{I}^{n,1} & \mathbf{I}^{n,n} \end{bmatrix} \begin{bmatrix} \boldsymbol{\Sigma}_{k|k-1}^{ss} & \boldsymbol{\Sigma}_{k|k-1}^{sd} \\ \boldsymbol{\Sigma}_{k|k-1}^{ds} & \boldsymbol{\Sigma}_{k|k-1}^{dd} \end{bmatrix} \begin{bmatrix} \mathbf{I}^{1,1} & -\mathbf{I}^{1,n} \\ \mathbf{0} & \mathbf{I}^{n,n} \end{bmatrix} \\
&\quad + \begin{bmatrix} \boldsymbol{\Sigma}_k^{\mathbf{v}^s} & \mathbf{0} \\ \mathbf{0} & diag\left\{ \boldsymbol{\Sigma}_k^{{}^s\mathbf{v}^{d_i}} \right\}_{i=1,\ldots,n} \end{bmatrix} \\
&= \begin{bmatrix} \mathbf{I}^{1,1} & \mathbf{0} \\ -\mathbf{I}^{n,1} & \mathbf{I}^{n,n} \end{bmatrix} \begin{bmatrix} \boldsymbol{\Sigma}_{k|k-1}^{ss} & \left[-\boldsymbol{\Sigma}_{k|k-1}^{ss} + \boldsymbol{\Sigma}_{k|k-1}^{sd_j} \right]_{i=1,\, j=1,\ldots,n} \\ \boldsymbol{\Sigma}_{k|k-1}^{ds} & \left[-\boldsymbol{\Sigma}_{k|k-1}^{d_i s} + \boldsymbol{\Sigma}_{k|k-1}^{d_i d_j} \right]_{i=1,\ldots,n,\, j=1,\ldots,n} \end{bmatrix} \\
&\quad + \begin{bmatrix} \boldsymbol{\Sigma}_k^{\mathbf{v}^s} & \mathbf{0} \\ \mathbf{0} & diag\left\{ \boldsymbol{\Sigma}_k^{{}^s\mathbf{v}^{d_i}} \right\}_{i=1,\ldots,n} \end{bmatrix} \\
&= \begin{bmatrix} \boldsymbol{\Sigma}_{k|k-1}^{ss} & \left[-\boldsymbol{\Sigma}_{k|k-1}^{ss} + \boldsymbol{\Sigma}_{k|k-1}^{sd_j} \right]_{i=1,\, j=1,\ldots,n} \\ \left[-\boldsymbol{\Sigma}_{k|k-1}^{ss} + \boldsymbol{\Sigma}_{k|k-1}^{d_i s} \right]_{i=1,\ldots,n,\, j=1,} & \left[\boldsymbol{\Sigma}_{k|k-1}^{ss} - \boldsymbol{\Sigma}_{k|k-1}^{sd_j} \right. \\ & \left. -\boldsymbol{\Sigma}_{k|k-1}^{d_i s} + \boldsymbol{\Sigma}_{k|k-1}^{d_i d_j} \right]_{i=1,\ldots,n,\, j=1,\ldots,n} \end{bmatrix} \\
&\quad + \begin{bmatrix} \boldsymbol{\Sigma}_k^{\mathbf{v}^s} & \mathbf{0} \\ \mathbf{0} & diag\left\{ \boldsymbol{\Sigma}_k^{{}^s\mathbf{v}^{d_i}} \right\}_{i=1,\ldots,n} \end{bmatrix}
\end{aligned}
$$

or, in the most compact form,

$$
\begin{aligned}
\mathbf{S}_k^{ss} &= \boldsymbol{\Sigma}_{k|k-1}^{ss} + \boldsymbol{\Sigma}_k^{\mathbf{v}^s} \\
\mathbf{S}_k^{sd} &= \left[-\boldsymbol{\Sigma}_{k|k-1}^{ss} + \boldsymbol{\Sigma}_{k|k-1}^{sd_j} \right]_{i=1,\, j=1,\ldots,n} \\
\mathbf{S}_k^{ds} &= \left[-\boldsymbol{\Sigma}_{k|k-1}^{ss} + \boldsymbol{\Sigma}_{k|k-1}^{d_i s} \right]_{i=1,\ldots,n,\, j=1} \\
\mathbf{S}_k^{dd} &= \left[\boldsymbol{\Sigma}_{k|k-1}^{ss} - \boldsymbol{\Sigma}_{k|k-1}^{sd_j} - \boldsymbol{\Sigma}_{k|k-1}^{d_i s} + \boldsymbol{\Sigma}_{k|k-1}^{d_i d_j} \right]_{i=1,\ldots,n,\, j=1,\ldots,n} + diag\left\{ \boldsymbol{\Sigma}_k^{{}^s\mathbf{v}^{d_i}} \right\}_{i=1,\ldots,n}
\end{aligned}
$$

Extension for Identification of Defects of Unknown Number

The exploration of a new area may results in identifying a defect that is not found in the current list. Assume that (n+1)th defect has been detected at the kth measurement with observation ${}^s\tilde{\mathbf{z}}_k^{d_{n+1}}$. Similarly to the other defects, the motion and the observation models of the defect are given by

$$
\begin{aligned}
\mathbf{x}_k^{d_{n+1}} &= \mathbf{x}_{k-1}^{d_{n+1}} \\
{}^s\mathbf{z}_k^{d_{n+1}} &= -\mathbf{x}_k^s + \mathbf{x}_k^{d_{n+1}} + {}^s\mathbf{v}_k^{d_{n+1}}
\end{aligned}
$$

where ${}^s\mathbf{v}_k^{d_{n+1}} \sim N\left(\mathbf{0}, \boldsymbol{\Sigma}_{{}_s\mathbf{v}_k^{d_{n+1}}}\right)$ may be a uniform distribution with large covariance. With no motion, the prediction is simply

$$\mathbf{x}_{k|k-1}^{d_{n+1}} = \mathbf{x}_{k-1|k-1}^{d_{n+1}}$$
$$\mathbf{\Sigma}_{k|k-1}^{d_{n+1}} = \mathbf{\Sigma}_{k-1|k-1}^{d_{n+1}}$$

The independence of the mean correction for each sensor and defect yields the mean correction for (n+1)th defect as

$$\overline{\mathbf{x}}_{k|k}^{d_{n+1}} = \overline{\mathbf{x}}_{k|k-1}^{d_{n+1}} + \mathbf{K}_k^{d_{n+1}s}\left(\tilde{\mathbf{z}}_k^s - \overline{\mathbf{x}}_{k|k-1}^s\right) + \sum_{j=1}^{n+1}\mathbf{K}_k^{d_{n+1}d_j}\left({}^s\tilde{\mathbf{z}}_k^{d_j} + \overline{\mathbf{x}}_{k|k-1}^s - \overline{\mathbf{x}}_{k|k-1}^{d_j}\right)$$

The correction of covariance, on the other hand, is conducted with all the sensor and defects. Let the matrix constructed with n defects be $(\cdot)^{nn}$, the matrices associated with (n+1)th defect be $(\cdot)^{++}$, $(\cdot)^{+n}$ and $(\cdot)^{n+}$. The correction of covariance is offered by

$$\begin{aligned}
&\begin{bmatrix} \mathbf{\Sigma}_{k|k}^{nn} & \mathbf{\Sigma}_{k|k}^{n+} \\ \mathbf{\Sigma}_{k|k}^{+n} & \mathbf{\Sigma}_{k|k}^{++} \end{bmatrix} \\
&= \left(\begin{bmatrix} \mathbf{I}^{1,1} & \mathbf{0} \\ \mathbf{0} & \mathbf{I}^{n,n} \end{bmatrix} - \begin{bmatrix} \mathbf{K}_k^{nn} & \mathbf{K}_k^{n+} \\ \mathbf{K}_k^{+n} & \mathbf{K}_k^{++} \end{bmatrix} \begin{bmatrix} \mathbf{C}_k^{n,n} & \mathbf{0} \\ \left[\mathbf{I}^{1,1}, \mathbf{0}, \ldots, \mathbf{0}\right] & \mathbf{I}^{1,1} \end{bmatrix} \right) \begin{bmatrix} \mathbf{\Sigma}_{k|k-1}^{nn} & \mathbf{\Sigma}_{k|k-1}^{n+} \\ \mathbf{\Sigma}_{k|k-1}^{+n} & \mathbf{\Sigma}_{k|k-1}^{++} \end{bmatrix} \\
&= \begin{bmatrix} \mathbf{I}^{n,n} - \mathbf{K}_k^{nn}\mathbf{C}_k^{nn} - \left[\mathbf{K}_k^{i+}, \mathbf{0}, \ldots, \mathbf{0}\right]_{i=1,\ldots,n} & -\mathbf{K}_k^{n+} \\ -\mathbf{K}_k^{+n}\mathbf{C}_k^{nn} - \left[\mathbf{K}_k^{++}, \mathbf{0}, \ldots, \mathbf{0}\right] & \mathbf{I}^{1,1} - \mathbf{K}_k^{++} \end{bmatrix} \begin{bmatrix} \mathbf{\Sigma}_{k|k-1}^{nn} & \mathbf{\Sigma}_{k|k-1}^{n+} \\ \mathbf{\Sigma}_{k|k-1}^{+n} & \mathbf{\Sigma}_{k|k-1}^{++} \end{bmatrix}
\end{aligned}$$

where the Kalman gain is computed from Eq. (\ref{eq:K}). The extraction of the update of

$$\begin{aligned}
\mathbf{\Sigma}_{k|k}^{nn} &= \mathbf{I}^{n,n} - \mathbf{K}_k^{nn}\mathbf{C}_k^{nn} - \left[\mathbf{K}_k^{i+}, \mathbf{0}, \ldots, \mathbf{0}\right]_{i=1,\ldots,n}\mathbf{\Sigma}_{k|k-1}^{nn} - \mathbf{K}_k^{n+}\mathbf{\Sigma}_{k|k-1}^{+n} \\
&= \left(\mathbf{I}^{n,n} - \mathbf{K}_k^{nn}\mathbf{C}_k^{nn}\right)\mathbf{\Sigma}_{k|k-1}^{nn} - \left\{\left[\mathbf{K}_k^{i+}, \mathbf{0}, \ldots, \mathbf{0}\right]_{i=1,\ldots,n}\mathbf{\Sigma}_{k|k-1}^{nn} + \mathbf{K}_k^{n+}\mathbf{\Sigma}_{k|k-1}^{+n}\right\}
\end{aligned}$$

most importantly describes that the covariance of the sensor and the present defects will be influenced by the newly detected defect.

Evaluation of identification

The uncertainty described by a covariance matrix can be represented by a single measure to quantify the result of identification. The measure proposed to quantify various uncertainties is the differential entropy, which describes the absolute value of uncertainty in continuous space and thus allows us to evaluate the identification result with a reliability criterion. One type of reliability criterion introduced using the differential entropy is the uncertainty of individual sensor or defect location:

$$H_k^s = \frac{1}{2}\ln\left\{(2\pi e)^{n_s}\det\mathbf{\Sigma}_k^{ss}\right\}$$
$$H_k^{d_i} = \frac{1}{2}\ln\left\{(2\pi e)^{n_s}\det\mathbf{\Sigma}_k^{d_i d_i}\right\}$$

where n_s is the number of state variables for a NDE sensor or a defect, since individual evaluation allows us to identify which individual is comparatively more uncertain than others. Another type of quantity proposed for evaluation is the differential entropy quantifying the uncertainties of all the sensor and defects, which is also defined as the total differential entropy:

$$H_k^n = \frac{1}{2}\ln\left\{(2\pi e)^{n \cdot n_s} \det \boldsymbol{\Sigma}_k^{nn}\right\}$$

This evaluates the overall performance of the identification.

Numerical Examples

This section investigates the performance of the proposed stochastic defect identification technique in two steps. The first step solves an algebraic problem that approximates a defect identification problem with different parameters (Tests 1-3) and analyzes the mechanisms of the proposed technique. After the parametric studies, the applicability of the proposed technique to the identification of defects is described in the second step (Test 4).

Concept Proving by Algebraic Problem

The defect identification problem defined for Tests 1-3 attempts to identify a single defect in a rectangular specimen by a NDE sensor. Figure 1 illustrates the setup of the defect identification test. A defect is located near the center of the specimen, and the NDE sensor moves linearly along the *x* direction across the specimen once approaching to the defect and then getting far away. The motion model of the NDE sensor in Equation is simplified as:

$$\mathbf{x}_k^s = \mathbf{x}_{k-1}^s + \mathbf{u}_k^s + \mathbf{w}_k^s$$

where $\mathbf{u}_k^s$ produces a positive linear increment in *x* component.

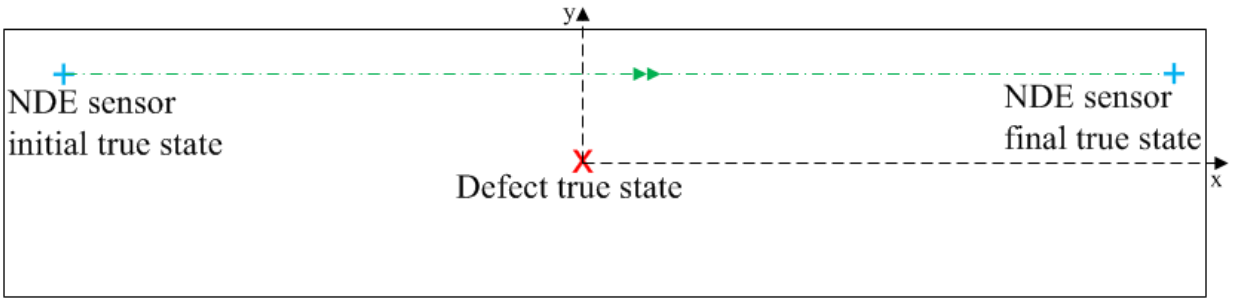

Figure 1 Setup of the defect identification for Tests 1-3.

Table 1 lists the parameters and formulations used commonly to create measurements in Tests 1-3. The measurements were created by firstly specifying the true state of the NDE sensor and the first defect and then adding noises with specified variances. The defect state used to create

measurements was $\mathbf{x}^{d1*} = [0,0]^\top$, so that it is expected that the proposed technique finds the defect around $\mathbf{x}^{d1*}$ while also identifying the sensor position appropriately. The system noise $\mathbf{w}_k^s$ and the observation noise for the sensor $\mathbf{v}_k^s$ were respectively given by diagonal matrices. As one of the simplest approximate implementations of the NDE sensor, which detect bearing more accurately than range, the observation noise for a defect has the covariance as:

$$\mathbf{\Sigma}_k^{{}^s\mathbf{v}^{d1}} = \alpha \begin{bmatrix} \cos\left({}^s\theta_k^d\right) & -\sin\left({}^s\theta_k^d\right) \\ \sin\left({}^s\theta_k^d\right) & \cos\left({}^s\theta_k^d\right) \end{bmatrix} diag\left\{2\,{}^sl_k^d,\, {}^sl_k^d\right\} \begin{bmatrix} \cos\left({}^s\theta_k^d\right) & -\sin\left({}^s\theta_k^d\right) \\ \sin\left({}^s\theta_k^d\right) & \cos\left({}^s\theta_k^d\right) \end{bmatrix}^{-1}$$

where ${}^sl_k^d$ and ${}^s\theta_k^d$ are the distance and the angle of the mean defect state based on the mean sensor state, α is a scaling factor, and 2 in the diagonal matrix makes the observation directional. Distance errors of the estimated identified defect and sensor states to their true states, given by

$$\text{DistanceError} = \left|\mathbf{x}_k^{(\cdot)} - \mathbf{x}_k^{(\cdot)*}\right|$$

are also utilized as one of the metrics to evaluate the performance of the proposed technique, where $(\cdot)$ is referring to either the identified defect or the sensor.

Table 2 Parameters and formulations commonly used to create measurements in Tests 1-3.

Parameter	True	Parameter	Proposed
$\mathbf{x}^{d1*\top}$	$[0,0]$	$\mathbf{\Sigma}_k^{d1d1}$	$diag\left\{\Sigma_{0x}^{d1d1}, \Sigma_{0y}^{d1d1}\right\}$
$\mathbf{x}_0^{s*\top}$	$[-10,1]$	$\mathbf{\Sigma}_k^{ss}$	$diag\left\{\Sigma_{0x}^{ss}, \Sigma_{0y}^{ss}\right\}$
$\mathbf{u}_k^{s*\top}$	$[1,0]$	$\mathbf{u}_k^{s\top}$	$[1,0]$
$\mathbf{\Sigma}_k^{\mathbf{w}^s*}$	$diag\left\{\Sigma_x^{\mathbf{w}^s*}, \Sigma_y^{\mathbf{w}^s*}\right\}$	$\mathbf{\Sigma}_k^{\mathbf{w}^s}$	$diag\left\{\Sigma_x^{\mathbf{w}^s*}, \Sigma_y^{\mathbf{w}^s*}\right\}$
$\mathbf{\Sigma}_k^{\mathbf{v}^s*}$	$diag\left\{\Sigma_x^{\mathbf{v}^s*}, \Sigma_y^{\mathbf{v}^s*}\right\}$	$\mathbf{\Sigma}_k^{\mathbf{v}^s}$	$diag\left\{\Sigma_x^{\mathbf{v}^s*}, \Sigma_y^{\mathbf{v}^s*}\right\}$
$\mathbf{\Sigma}_k^{{}^s\mathbf{v}^{d1}*}$	Eq of observation noise	$\mathbf{\Sigma}_k^{{}^s\mathbf{v}^{d1}}$	Eq of observation noise

Transitional performance (Test 1)

In order to investigate its transitional performance and the mechanism of estimation, the proposed technique was first applied to estimating the defect with three different sets of prior and empirical knowledge of the sensor. Table 3 shows all the prior and the empirical knowledge used in the three cases. In Case 1, the state of the NDE sensor was assumed to be precisely known, thus setting the mean of its prior knowledge to the true state $\mathbf{x}_0^s = \mathbf{x}_0^{s*}$, the variances of its prior knowledge to all near-zero $\mathbf{\Sigma}_0^{ss} \approx \mathbf{0}$ and the variances of the empirical knowledge to all near-zero $\mathbf{\Sigma}_k^{\mathbf{w}^s} = \mathbf{\Sigma}_k^{\mathbf{v}^s} \approx \mathbf{0}$. Case 2 had uncertainties in the prior and the empirical knowledge on

the NDE sensor but they are smaller than those of the defect whereas the uncertainties of the NDE sensor were higher than those of the defect in Case 3. Since the prior calibration generally gives accurate statistical knowledge, the same covariances were used to create measurements.

Table 3 Parameters in Test 1

Parameter	True	Parameter	Case 1	Case 2	Case 3
		$\left(\overline{\mathbf{x}}_0^{d_1}\right)^\top$	$[1,1]$	$[1,1]$	$[1,1]$
		$\left[\Sigma_{0x}^{d_1 d_1}, \Sigma_{0y}^{d_1 d_1}\right]$	$[3,3]$	$[3,3]$	$[3,3]$
		$\left(\overline{\mathbf{x}}_0^{s}\right)^\top$	$[-10,1]$	$[-11,2]$	$[-11,2]$
		$\left[\Sigma_{0x}^{ss}, \Sigma_{0y}^{ss}\right]$	$[10^{-3},10^{-3}]$	$[1,1]$	$[4,4]$
$\left[\Sigma_x^{\mathbf{w}^s *}, \Sigma_y^{\mathbf{w}^s *}\right]$	$\left[\Sigma_x^{\mathbf{w}^s}, \Sigma_y^{\mathbf{w}^s}\right]$	$\left[\Sigma_x^{\mathbf{w}^s}, \Sigma_y^{\mathbf{w}^s}\right]$	$[10^{-3},10^{-3}]$	$[0.25,0.25]$	$[1,1]$
$\left[\Sigma_x^{\mathbf{v}^s *}, \Sigma_y^{\mathbf{v}^s *}\right]$	$\left[\Sigma_x^{\mathbf{v}^s}, \Sigma_y^{\mathbf{v}^s}\right]$	$\left[\Sigma_x^{\mathbf{v}^s}, \Sigma_y^{\mathbf{v}^s}\right]$	$[10^{-3},10^{-3}]$	$[0.25,0.25]$	$[1,1]$
$\alpha *$	1	α	1	1	1

Figures 2(a) and 2(b) show the transitions of the distance errors of the identified defect and sensor states to their true states in Cases 1-3 while the transitions of the computed variances of the defect and the sensor are shown in Figures 3(a) and 3(b). The results first show that the identified defect state converges toward the true state as the number of measurements acquired increases no matter what the sensor uncertainties are, indicating the ability of the proposed technique in handling sensor uncertainties. Meanwhile, the results also show a slower convergence rate and a higher distance error with larger sensor uncertainties, which is largely due to the error of estimating the sensor state resulting from the sensor uncertainties. The effectiveness of the proposed technique can be additionally understood from the transition of the computed variances of the defect and sensor. The variances of the defect keeps decreasing with increase in the number of measurements in all the cases even after the sensor approached the defect most closely at the 11th measurement. This is because the defect identification is carried out by correction with no prediction and thus does not propagate uncertainty regardless of the distance of the sensor to the defect. The variances in Case 1 particularly approaches zero due to the the absence of sensor uncertainties. The variances of the sensor, on the other hand, can increase as the result of Case 3 notably depicts since the motion model increases the variances. These results indicate that the variances of each defect and sensor are independently controlled by its own prediction whilst the correction interactively influences the variances.

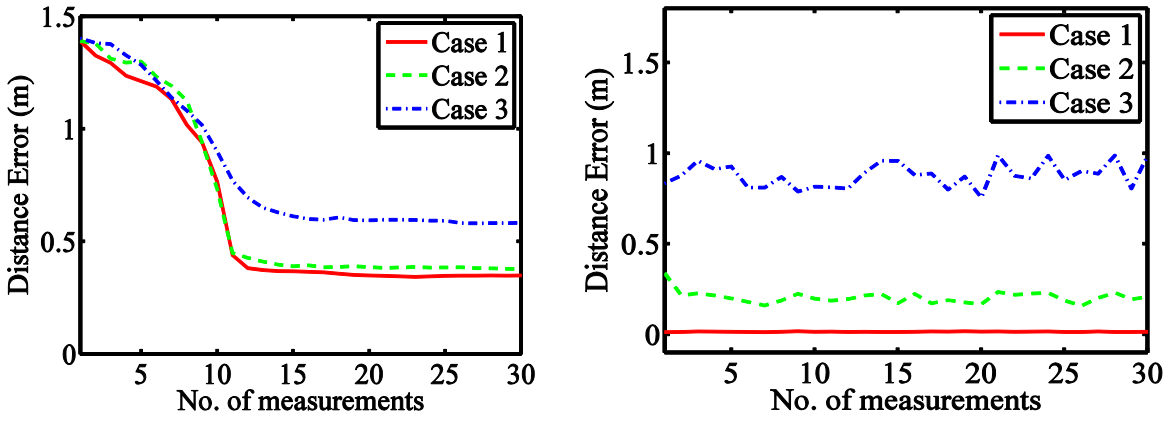

Figure 2 Identified means vs. measurements in Test 1

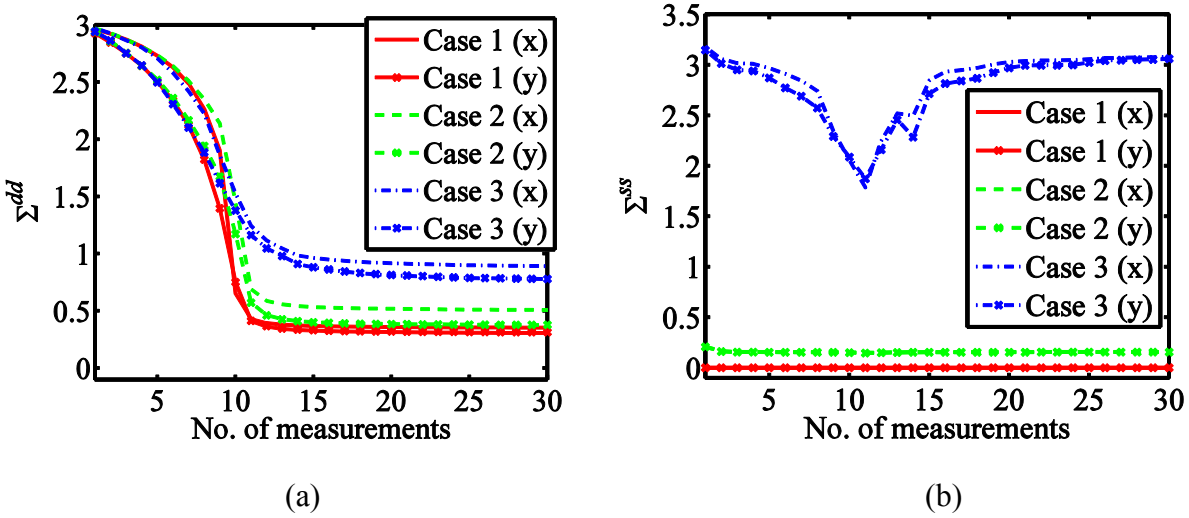

Figure 3 Computed variances vs. measurements in Test 1.

Figures 4 show the individual differential entropies of the defect and the NDE sensor and the total differential entropy in Cases 1–3. Since the differential entropy is a quantity extracted from variances, the behavior of the differential entropy inherits that of variances. Note that the negative values for differential entropy of the sensor of Case 1 are resulted from substitution of $\boldsymbol{\Sigma}^{ss} \approx \mathbf{0}$. Nevertheless, the quantification of uncertainty by a scalar value clearly makes the differential entropy useful and valuable as one can, for instance, judge the completion of a defect identification test based on the value of the differential entropy. If the reliability of the defect identification is only concerned, the differential entropy of the defect H_d may be the reference entropy. If the optimal sensor control is pursued for maximally reliable defect identification, total differential entropy H may be considered.

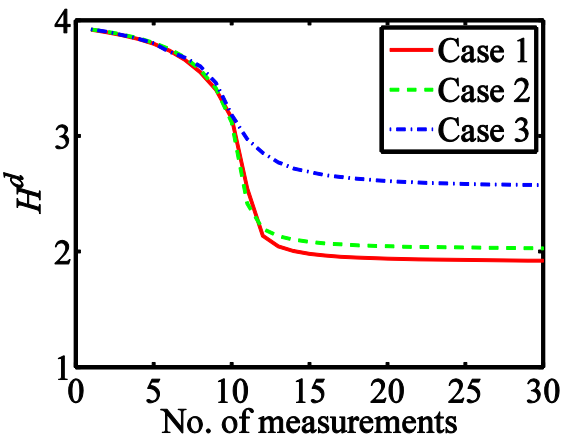

(a)

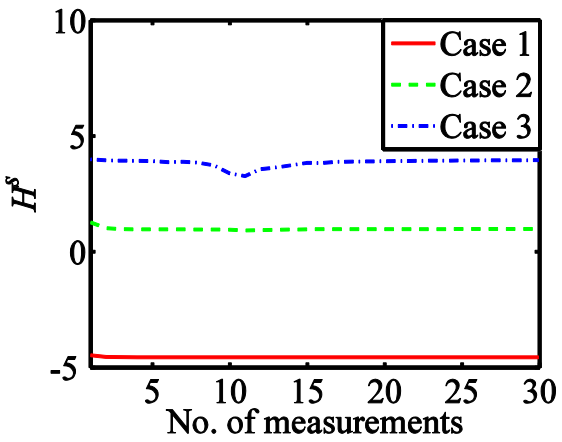

(b)

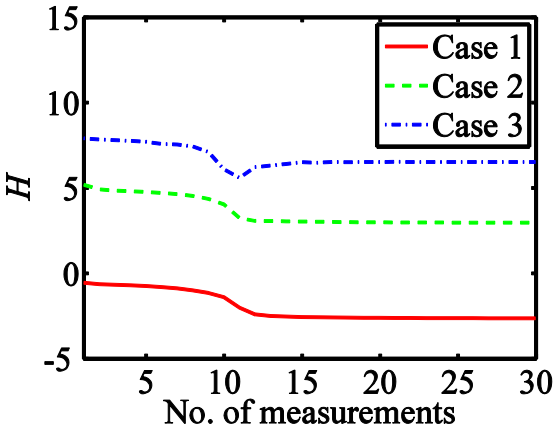

(c)

Figure 4 Differential entropies vs. measurements in Test 1

Effect of sensor uncertainties (Test 2)

Having understood its mechanisms of performance and effectiveness in more detail, the performance of the proposed technique was next investigated by solving estimation problems each with a different set of sensor uncertainties. Table 4 lists the parameters used to identify the defect by the proposed technique. The prior and the empirical knowledge on the NDE sensor were varied within the range specified by $\forall x$ and $\forall y$ while the number of measurements was set to 15. Due to the variation, it is possible to investigate the influence of the prior and the empirical knowledge on the proposed technique. The maximum limits of the prior and the empirical knowledge of the sensor were both set to 10 to comparatively investigate the influence of the prior and the empirical knowledge.

Table 4 Parameters in Test 2 $\left(\forall x \in [0.25,10], \forall y \in [0.25,10]\right)$

Parameter	True	Parameter	Case 1
		$\left(\bar{\mathbf{x}}_0^{d_1}\right)^\top$	$[1,1]$
		$\left[\Sigma_{0x}^{d_1 d_1}, \Sigma_{0y}^{d_1 d_1}\right]$	$[3,3]$
		$\left(\bar{\mathbf{x}}_0^{s}\right)^\top$	$[-10,1]$
		$\left[\Sigma_{0x}^{ss}, \Sigma_{0y}^{ss}\right]$	$[x,x]$
$\left[\Sigma_x^{\mathbf{w}^s *}, \Sigma_y^{\mathbf{w}^s *}\right]$	$[10^{-3}, 10^{-3}]$	$\left[\Sigma_x^{\mathbf{w}^s}, \Sigma_y^{\mathbf{w}^s}\right]$	$[10^{-3}, 10^{-3}]$
$\left[\Sigma_x^{\mathbf{v}^s *}, \Sigma_y^{\mathbf{v}^s *}\right]$	$\left[\Sigma_x^{\mathbf{v}^s}, \Sigma_y^{\mathbf{v}^s}\right]$	$\left[\Sigma_x^{\mathbf{v}^s}, \Sigma_y^{\mathbf{v}^s}\right]$	$[y,y]$
$\alpha *$	1	α	1

Figures 5(a)-5(c) show the distribution of the individual and total differential entropies with varying prior and empirical knowledge on the NDE sensor, whilst Figure 5(d) shows the distribution of the distance error of the identified defect state to the true defect state. The results first show the increase of all the individual and total differential entropies with respect to the increase of both the prior and the empirical knowledge. The prior knowledge has much less influence since the empirical knowledge has updated it 15 times, and its effect appears only when the empirical knowledge is uncertain. The increase of not only the differential entropy of the sensor H^s but also that of the defect H^d is due to the interactive influence of the covariances of the defect and the sensor. The identified defect state has a larger distance error when the empirical knowledge is more uncertain, but more certain prior knowledge caused a larger error due to its wrongness. The result concludes that the accuracy of identification drops in addition to the reliability when the empirical knowledge is uncertain.

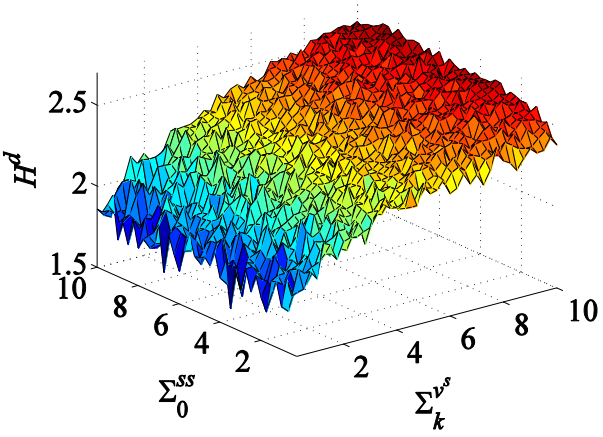

(a)

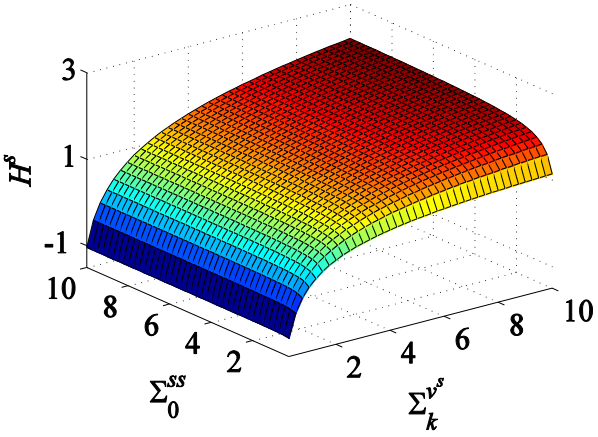

(b)

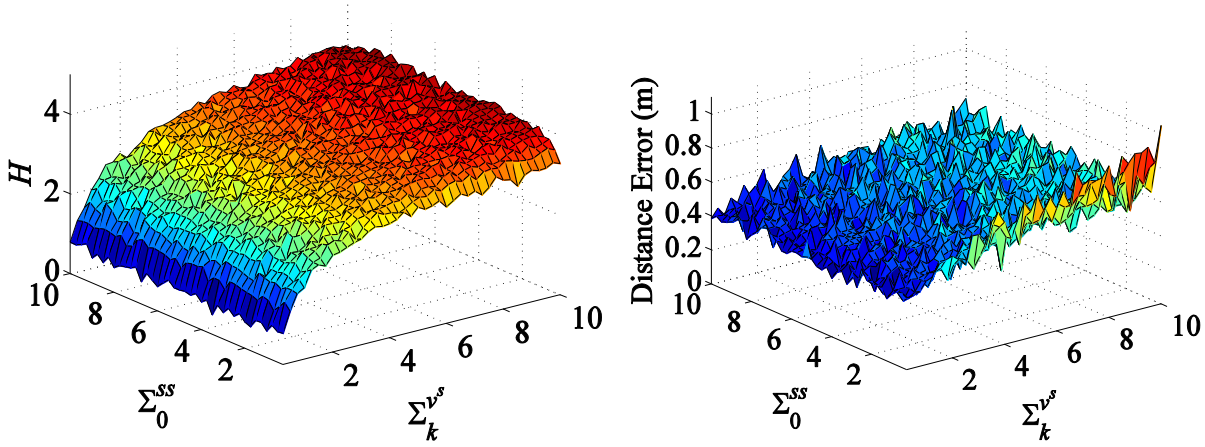

(c) (d)

Figure 5 Differential entropies and distance errors vs. sensor uncertainties in Test 2.

Effect of defect uncertainties (Test 3)

In this subsection, the ability of the proposed technique for identification under different defect uncertainties was investigated. Table 5 lists the parameters of the parametric study where the prior and the empirical knowledge on the defect, $\mathbf{\Sigma}_0^{d_1 d_1}$ and $\mathbf{\Sigma}_k^{s\mathbf{v}^{d_1}}$ were varied while those of the NDE sensor were fixed. Note that $\mathbf{\Sigma}_0^{d_1 d_1}$ was modified within the range specified by $\forall x$ and $\mathbf{\Sigma}_k^{s\mathbf{v}^{d_1}}$ was varied using substitution of α, which was differed within the range specified by $\forall y$, into the observation noise equation. Similarly to the previous test, identification results after 15 measurements were investigated.

Table 5 Parameters in Test 3 $\left(\forall x \in [0.25,10], \forall y \in [0.1,2]\right)$

Parameter	True	Parameter	Case 1
		$\left(\overline{\mathbf{x}}_0^{d_1}\right)^\top$	$[1,1]$
		$\left[\Sigma_{0x}^{d_1 d_1}, \Sigma_{0y}^{d_1 d_1}\right]$	$[x,x]$
		$\left(\overline{\mathbf{x}}_0^{s}\right)^\top$	$[-10,1]$
		$\left[\Sigma_{0x}^{ss}, \Sigma_{0y}^{ss}\right]$	$[1,1]$
$\left[\Sigma_x^{\mathbf{w}^s *}, \Sigma_y^{\mathbf{w}^s *}\right]$	$[10^{-3}, 10^{-3}]$	$\left[\Sigma_x^{\mathbf{w}^s}, \Sigma_y^{\mathbf{w}^s}\right]$	$[0.25,0.25]$
$\left[\Sigma_x^{\mathbf{v}^s *}, \Sigma_y^{\mathbf{v}^s *}\right]$	$\left[\Sigma_x^{\mathbf{v}^s}, \Sigma_y^{\mathbf{v}^s}\right]$	$\left[\Sigma_x^{\mathbf{v}^s}, \Sigma_y^{\mathbf{v}^s}\right]$	$[0.25,0.25]$
$\alpha *$	1	α	y

Figures 6(a) and 6(b) show the distributions of the differential entropy of the defect and the distance error with varying prior and empirical knowledge on the defect. Similarly to the study varying prior and empirical knowledge on the sensor, the differential entropy increases as uncertainty in the prior and empirical knowledge on the defect increases while the distance error increases in empirical knowledge and decreases in prior knowledge. The result, together with the result in Test 2 suggests that the defect identification be completed after the defect differential entropy has dropped and reached a specified value after the empirical knowledge, with enough measurements, has dominated the identification.

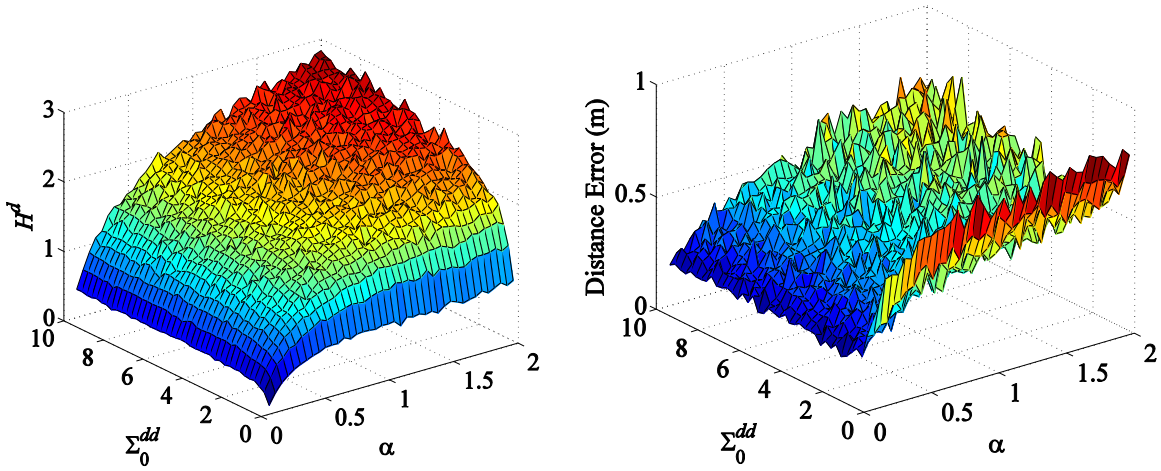

(a) (b)

Figure 6 Defect differential entropy and distance errors vs. defect uncertainties in Test 3.

Application to Non-destructive Evaluation (Test 4)

Since the number of defects in a practical scenario could be multiple and is unknown, the scenario of this subsection has located multiple defects in a square test specimen. Figure 7 shows the test specimen and the practical setup of the non-destructive evaluation. Three defects were located in a wide area to further resemble a practical problem where the defects are to be identified through search. In order to measure the sensor location with uncertainties most easily, a global camera was attached to view the sensor location over the entire test specimen. Based on the standard instructions, the transducer was slid on the specimen using the creeping line search pattern to search for defects and identified the location of each defect once it has been detected by the transducer. In an attempt to identify the defect location most reliably, or reduce the value of defect differential entropy, the identified defect was surrounded in a square motion. The surrounding motion continued until its differential entropy had reached a predetermined threshold value.

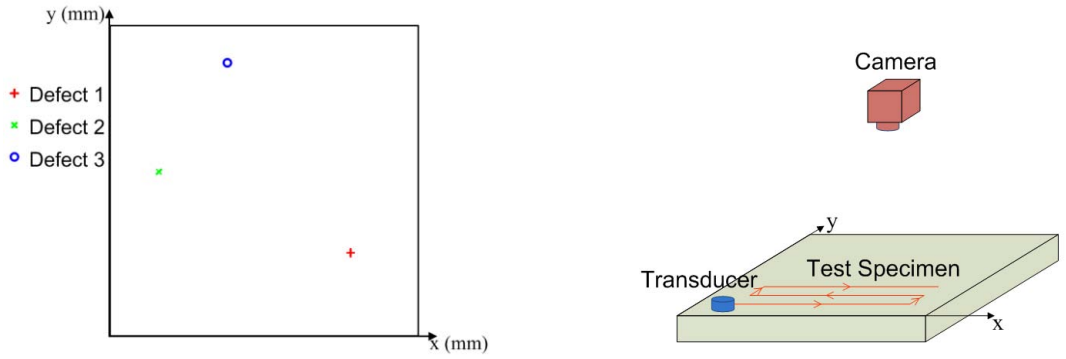

(a) (b)

Figure 7 Test specimen and experimental setup in Test 4.

Table 6 lists the parameters used to create measurements as well as the prior knowledge, the empirical knowledge and the threshold value of defect differential entropy used by the proposed technique. In order to demonstrate its wide applicability to defect identification, the prior knowledge of only the second defect was assumed to be known. It is to be noted that $\boldsymbol{\Sigma}_k^{w^{s*}} = \mathbf{0}$ and $\boldsymbol{\Sigma}_k^{v^{s*}} = \text{Const}$ since the global camera usage makes the estimation of the sensor location only through correction with fixed variances of the observation model.

Table 6 Parameters in Test 4

Parameter	True	Parameter	Proposed
$\mathbf{x}^{d_1 *\top}$	$[78,27],[16,53],[38,88]$	$\left(\bar{\mathbf{x}}_0^{d2}\right)^\top$	$[18,50]$
$\mathbf{x}_0^{s*\top}$	$[10,10]$	$\boldsymbol{\Sigma}_0^{d_2 d_2}$	$diag\{150,150\}$
$\mathbf{u}_k^{s*\top}$	$[5,0]$	$\boldsymbol{\Sigma}_0^{ss}$	$diag\{10,10\}$
$\boldsymbol{\Sigma}_k^{w^s *}$	$diag\{0,0\}$	$\left(\bar{\mathbf{u}}_k^s\right)^\top$	$[5,0]$
$\boldsymbol{\Sigma}_k^{v^s *}$	$diag\{10,10\}$	$\boldsymbol{\Sigma}_k^{v^s}$	$diag\{10,10\}$
$\boldsymbol{\Sigma}_k^{s\mathbf{v}^{d1}*}, \forall i \in \{1,\ldots,3\}$	Eq of observation noise	$\boldsymbol{\Sigma}_k^{s\mathbf{v}^{d1}*}, \forall i \in \{1,\ldots,3\}$	Eq of observation noise
		H_{thres}^d	3

Figure 8(a) shows the path of the transducer motion where the transducer has covered the entire specimen and detected and surrounded all the three defects. Shown in Figure 8(b), meanwhile, is the transition of the defect differential entropies as well as the vertical lines each exhibiting the completion of identification of a defect. It is first seen that the proposed technique can identify defects regardless of the availability of prior knowledge. The result also shows that the

differential entropies drop significantly by the square motion after detection. In addition, all the defect differential entropies are seen to keep decreasing irrespective of the sensor location owing to the stochastic identification. Figure 8(c) shows the resulting transition of the distance error of each identified defect to its true location. The identified defect locations well match with the true locations and, similarly to the differential entropies, the identified defect locations are continuously accurate regardless of the sensor location although their behavior is noisier.

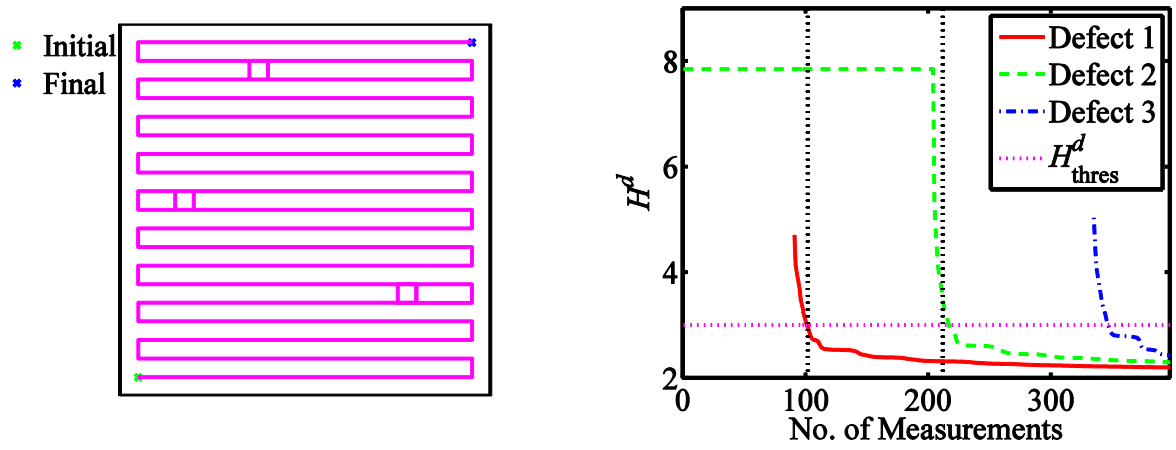

(a) (b)

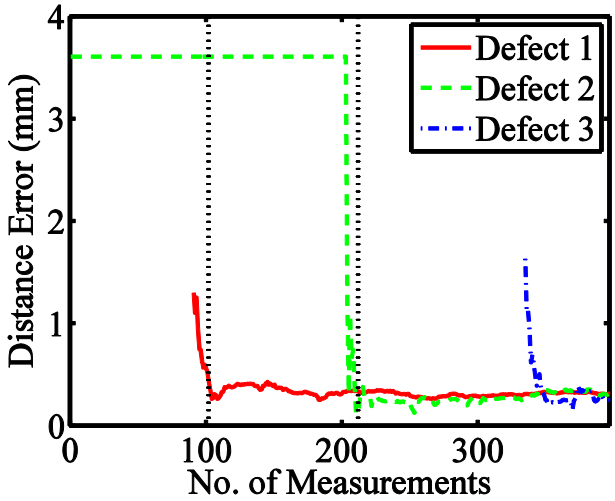

(c)

Figure 8 Resulting path, defect differential entropies and distance errors in Test 4

Rapid field inspection by optimally guiding and controlling sensors

A new framework to identify defects under the presence of sensor uncertainties has been developed, where the framework represents the beliefs of defects and sensor location by a

probabilistic density function and updates them in time and measurement using extended Kalman filter (EKF). Figure 9 presents the architecture of the theoretical framework, where the framework is divided into two processes, which are the deterministic and stochastic processes. The deterministic process begins with an inspector starting the sensor motion. This is modeled by a motion model to determine the estimated sensor location prior the current measurement $\mathbf{x}_k^s$, where this model is based on the uncertainty by the sensor motion and sensor location of the previous measurement. The $\mathbf{x}_k^s$ then acts as the input to determine the sensor estimated location prior the following measurement using the same motion model. Concurrently, the location $\mathbf{x}_k^s$ is utilized to model the measured defect and sensor locations ${}^s\tilde{\mathbf{z}}_k^{d_i}$ and $\tilde{\mathbf{z}}_k^s$ using two different sensor models. The location ${}^s\tilde{\mathbf{z}}_k^{d_i}$ is determined by a wave signal sensor model that utilizes a database developed using Finite Element Analysis (FEA) while location $\tilde{\mathbf{z}}_k^s$ is given by a camera sensor model. In the stochastic process, the belief of the sensor, which is represented by a mean and covariance, is first computed by the prediction formulations of EKF based on the sensor motion model, the uncertainty by the sensor motion represented by covariance $\boldsymbol{\Sigma}_k^{\mathbf{w}^s}$ and prior knowledge of the sensor $\bar{\mathbf{x}}_0^s$ and $\boldsymbol{\Sigma}_0^s$. The beliefs of the defects and sensor are then updated by the correction formulations of EKF using observations and their empirical knowledge $\boldsymbol{\Sigma}_k^{{}^s\mathbf{v}^{d_i}}$ and $\boldsymbol{\Sigma}_k^{\mathbf{v}^s}$, prior knowledge of the defects $\bar{\mathbf{x}}_0^{d_i}$ and $\boldsymbol{\Sigma}_0^{d_i}$, and previously determined belief of the sensor from the prediction formulations. The resultant beliefs of the defects and sensor, collectively as $\bar{\mathbf{x}}_{k|k}$ and $\boldsymbol{\Sigma}_{k|k}$, are then utilized as the past beliefs for the update in time and measurement of the following sensor motion and observations. The covariance $\boldsymbol{\Sigma}_{k|k}$ is also quantified to differential entropy H and guides the inspector for the next sensor motion. The rapid field inspection is repeated until the differential entropy is below a set threshold.

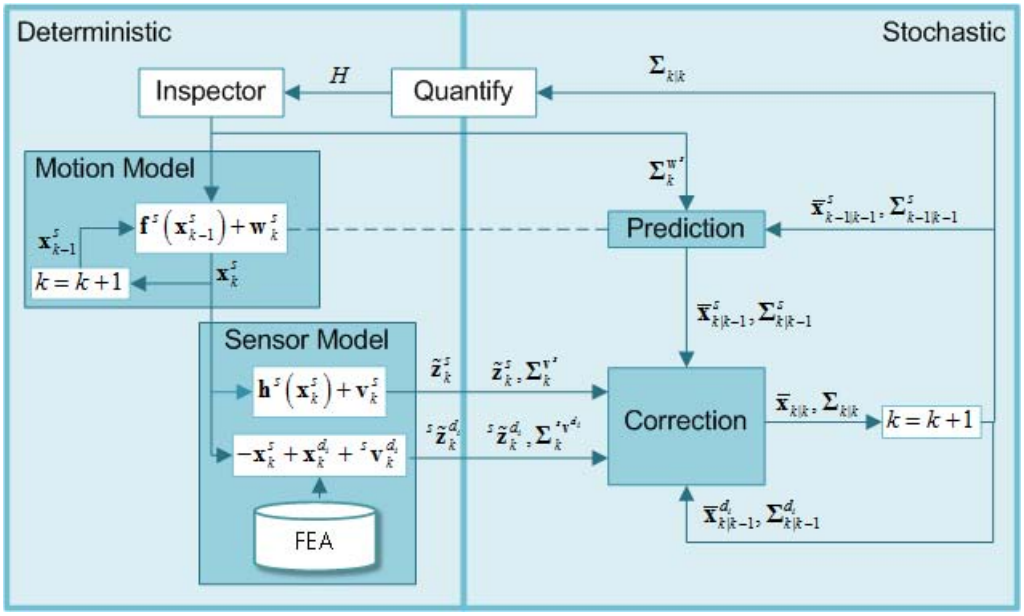

Figure 9 The architecture of the theoretical framework

Since the beliefs are recursively maintained during the sensor motion and observations, the proposed framework considers not only the current observation but also the prior knowledge, the past beliefs and the past observations. In addition, the beliefs of the defect and the sensor are updated concurrently and interactively and thus allow identification under sensor uncertainties.

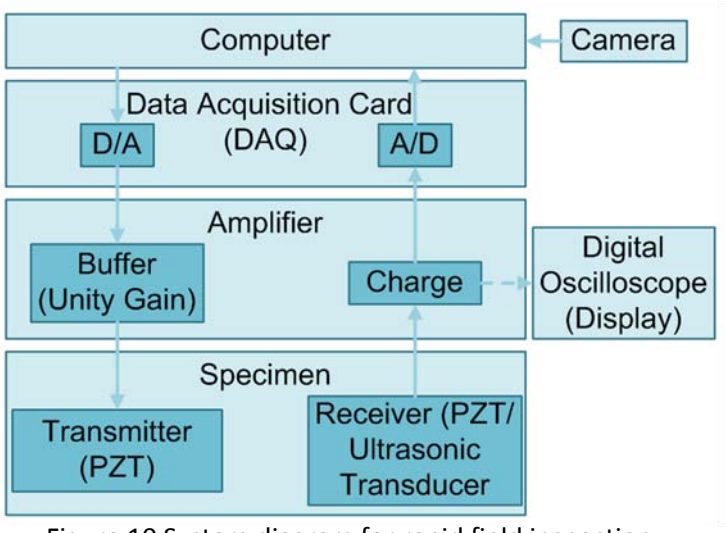

Figure 10 System diagram for rapid field inspection

Figure 10 shows the system diagram of the rapid field inspection, noting the required instruments and connection between them. The computer generates the signal for transmitter excitation and is amplified using the buffer amplifier prior sending to the PZT, which is acting as a transmitter. The signal from the receiver, which is either another PZT or an ultrasonic transducer, is amplified using a charge amplifier before being analyzed by the signal analysis in the computer. Concurrently, the position of the receiver is monitored by the camera. The validity of the signal from the receiver is verified by the digital oscilloscope. Figure 11 shows the experimental setup for the rapid field inspection and based on the system diagram.

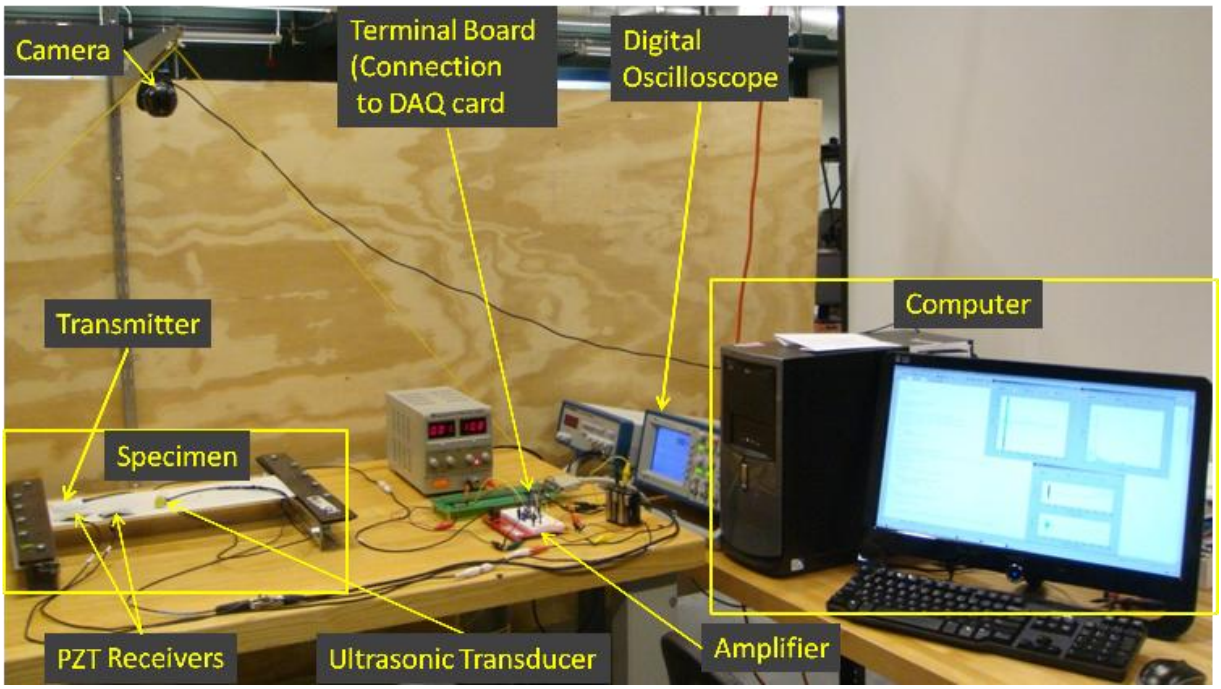

Figure 11 The experiment setup for rapid field inspection

Defect, transmitter and receiver layouts on the specimen

Figure 12 shows the defect and transmitter positions of the specimen as well as the size of the specimen while Figure 13 illustrates the example of the transmitter and receiver layouts on the specimen for the rapid field inspection framework, where two different receiver layout sets are given in Table 7.

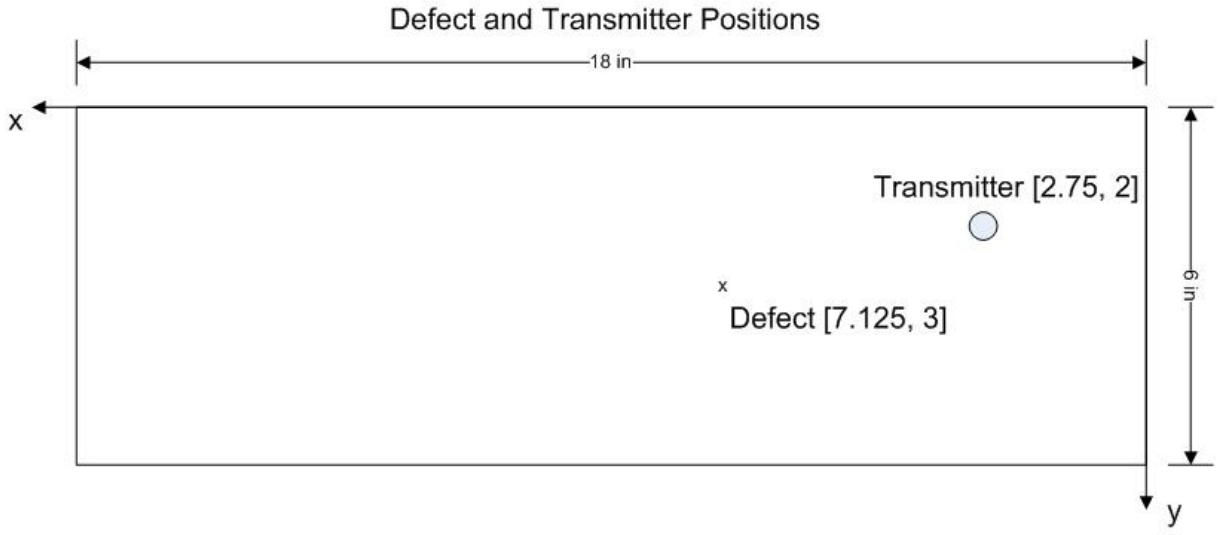

Figure 12 Defect and transmitter positions on the specimen

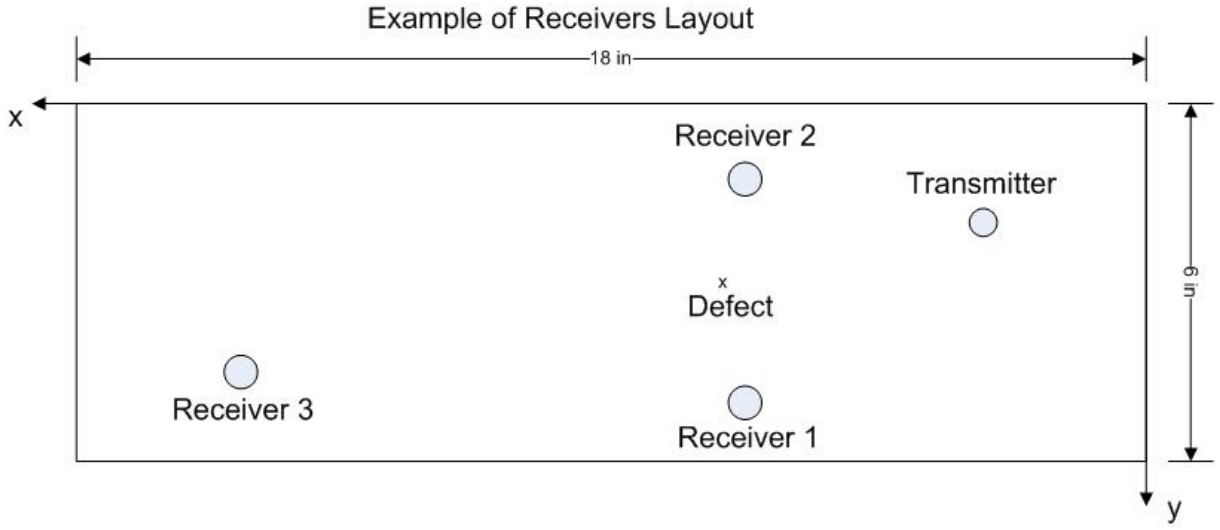

Figure 13 Example of receivers' position layouts on the specimen

Table 7 Receivers' position layout on the specimen

	Receiver 1	Receiver 2	Receiver 3
Layout 1	[7, 3.75]	[7, 2.125]	[8.75, 2.75]
Layout 2	[6.75, 5]	[6.75, 1.25]	[15.25, 4.5]

The position of the defect is evaluated based on the signal analysis of the signals from the transmitter and receivers using an appropriate filter. Figure 14 shows the comparison between three different filters, which are Butterworth, Elliptic and Chebyshev II filters. Based on this analysis, it is shown that the Elliptic signal is the preferred choice due to its capability to reduce the 'overturn' effect shown in the Butterworth and Chebyshev II filters.

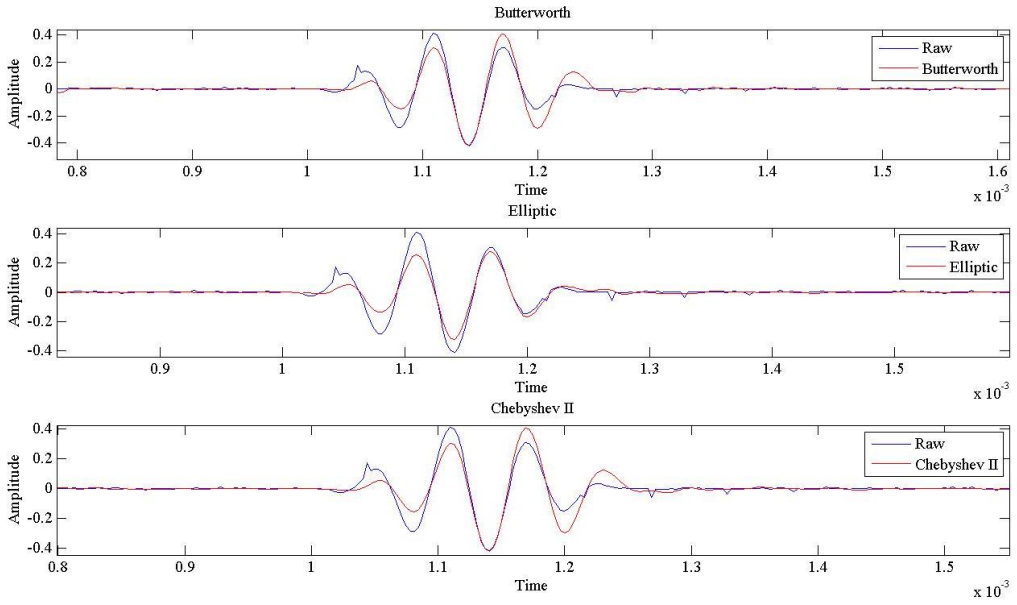

Figure 14 Comparison between different filters

Figures 15 and 16 show the evaluation of the defect existence and distance approximation of the defect position based on the receiver. As shown in Figure 15, there is a time lag between the signals from the transmitter and receivers. This is better shown in Figure 16, and the time difference is used as a factor with the sampling frequency of the receiver and transmitter as well as the speed of sound of the specimen materials.

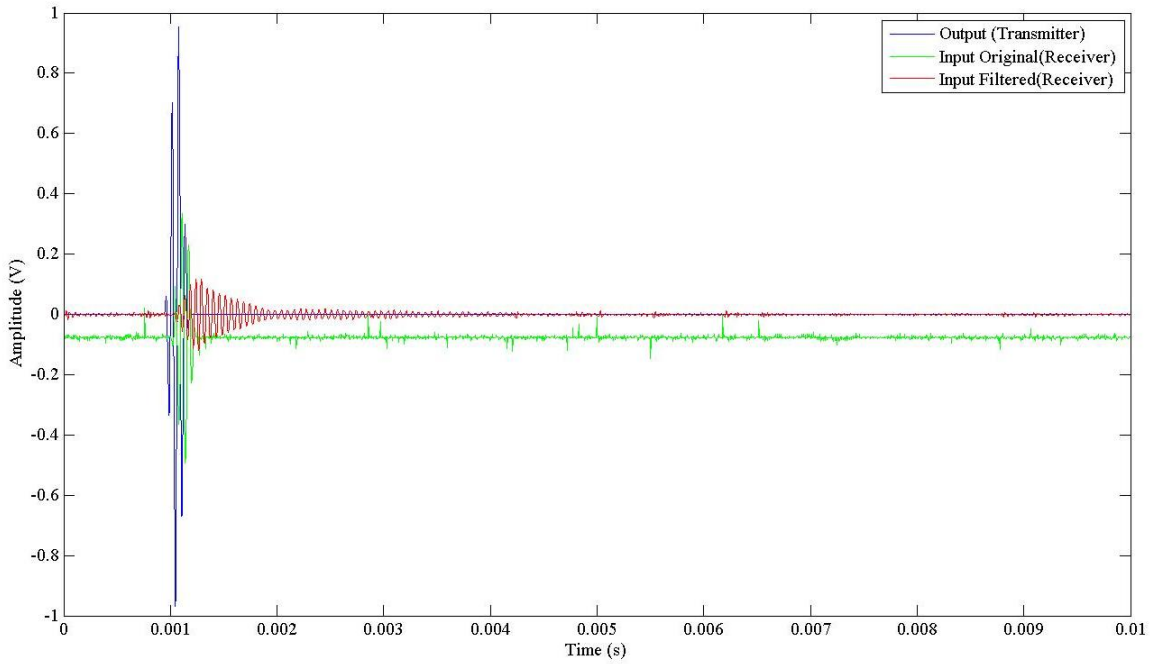

Figure 15 Evaluation of the defect existence based on the transmitter and receiver signals

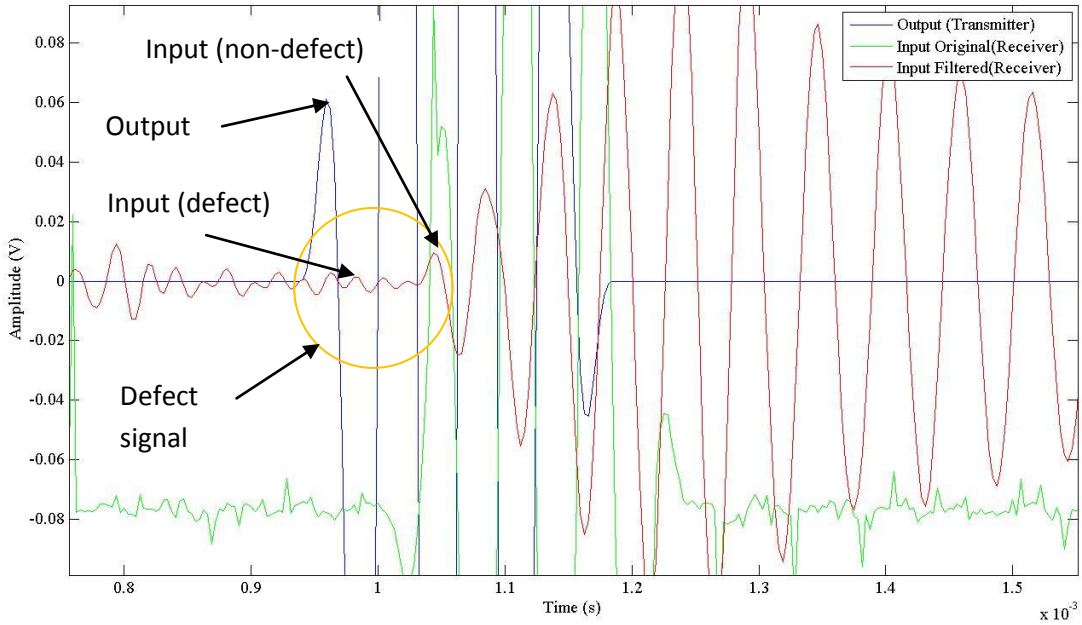

Figure 16 The difference between 'with' and 'without defect' signals

Implementation of the rapid field inspection

With the given capability to determine the position of the defects, this subsection shows the implementation of the rapid field inspection. In this implementation, a transmitter and three static receivers are utilized to provide the prior knowledge of the position and number of defects on the specimen. The rapid field inspection is applied using an ultrasonic transducer to provide a better position estimation of the defects, where the position of the ultrasonic transducer is estimated by a camera system shown in Figure 11 and the implementation aims to reduce the covariance to a few certain differential entropy thresholds. Figure 17 shows the initial setup of the rapid field inspection, where Figure 17(a) depicts the position of the transmitter, which is appointed with green paper and the static receivers, which are given by the orange papers, and also the prior knowledge of the identified defects, which are marked as blue color. This figure shows that three defects are identified. Meanwhile, Figure 17(b) shows the estimated position of the ultrasonic transducer, which are marked as magenta color. The red color indicates the targeted defects to be provided better estimation using the ultrasonic transducer and implemented rapid field inspection. The rapid field inspection consists of two phases:

1) Reduction of all the defects differential entropy to meet the first differential entropy threshold

2) Traversing motion of the transducer to further reduce all the defects differential entropy to meet the second differential entropy threshold.

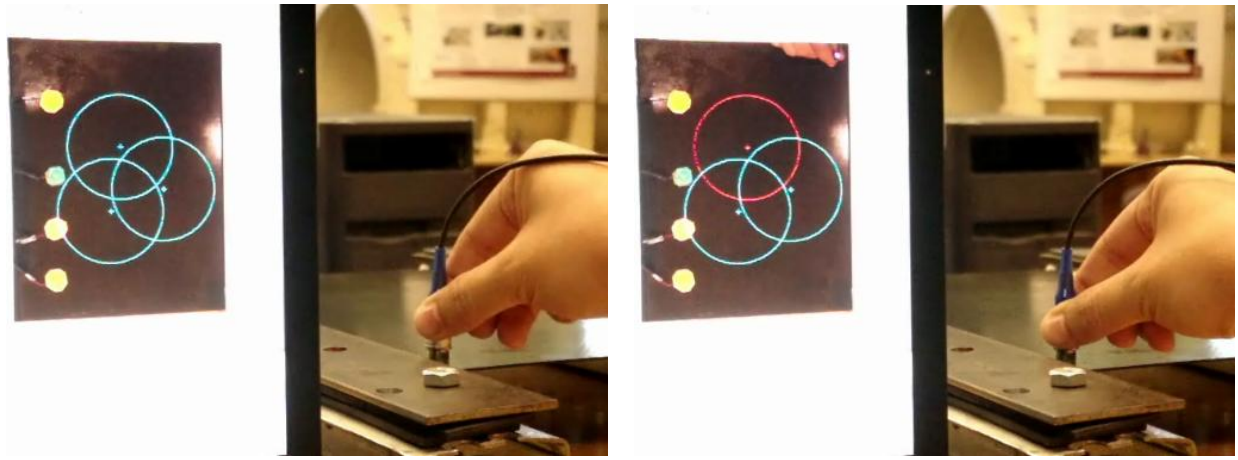

(a) (b)

Figure 17 The initial setup of the rapid field inspection implementation.

Figure 18 shows the sequential steps of the rapid field implementation. Figures 18(a) indicates the motion of the transducer and this motion provide a better estimation and covariance of the first targeted defect, as illustrated by the covariance size difference of the targeted defect when compared with other defects. Figure 18(b) shows that the covariance of the first defect has met the first differential entropy threshold and the estimated position and covariance has changed to green color, and once this threshold is met, the ultrasonic transducer changed its target to next defect.

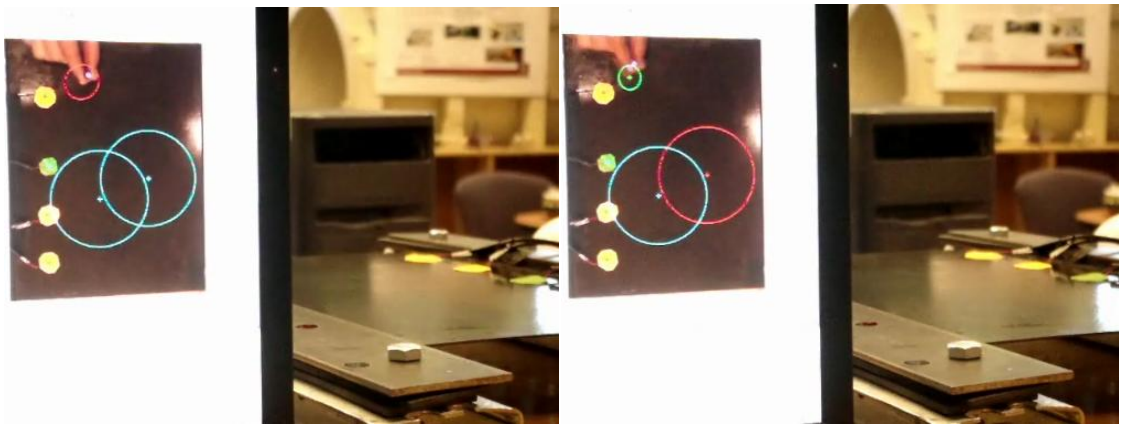

(a) (b)

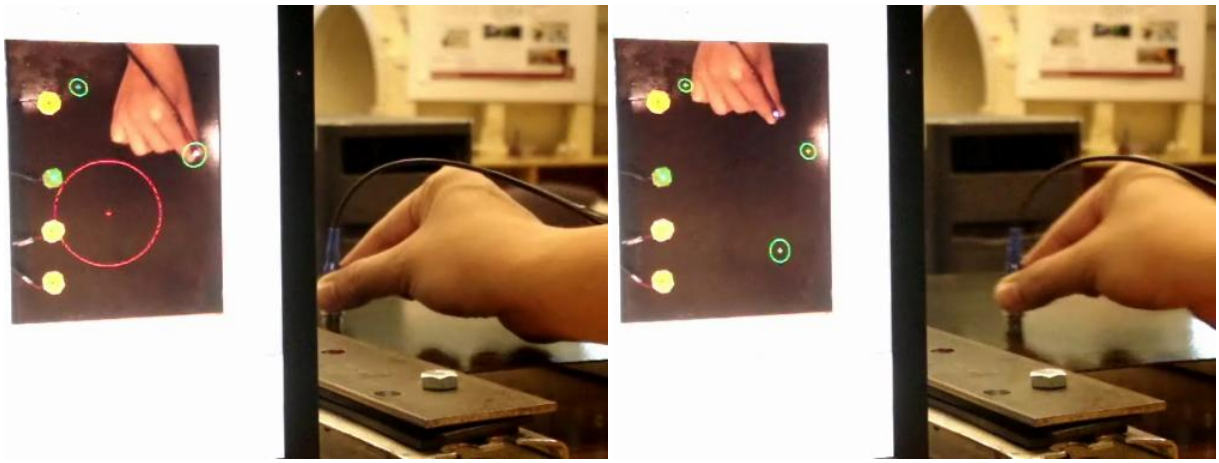

(c) (d)

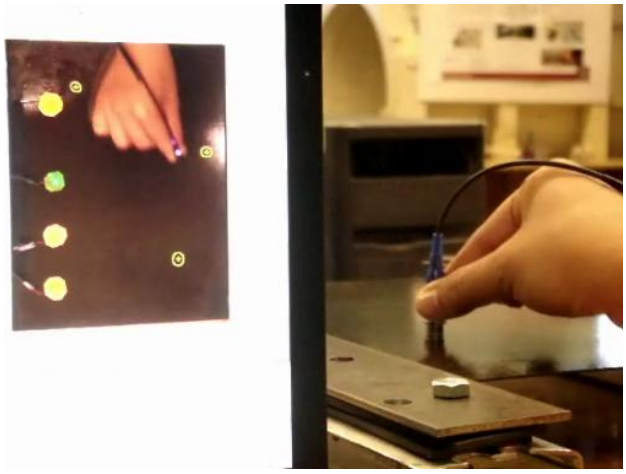

(e)

Figure 18 The steps of the rapid field inspection implementation.

The same step applied to the first targeted defect is used to estimate the remaining defects to the first differential entropy threshold (green), as shown in Figure 18(c). Figure 18(d) illustrates the beginning of the traversing motion of the ultrasonic transducer when all the defects covariance have met the first differential entropy threshold. This traversing motion is utilized to further improve the estimation of the defects to meet the second differential entropy threshold. The completion of the rapid field inspection, which is illustrated in Figure 18(e), is achieved when all the defects covariance met the second differential entropy threshold, which is indicated by yellow color. Figure 19 shows the differential entropy transitions of the multiple defects based on the rapid field inspection implementation. Here, it is shown that the first and second differential entropy threshold are set as 11.6 and 7.

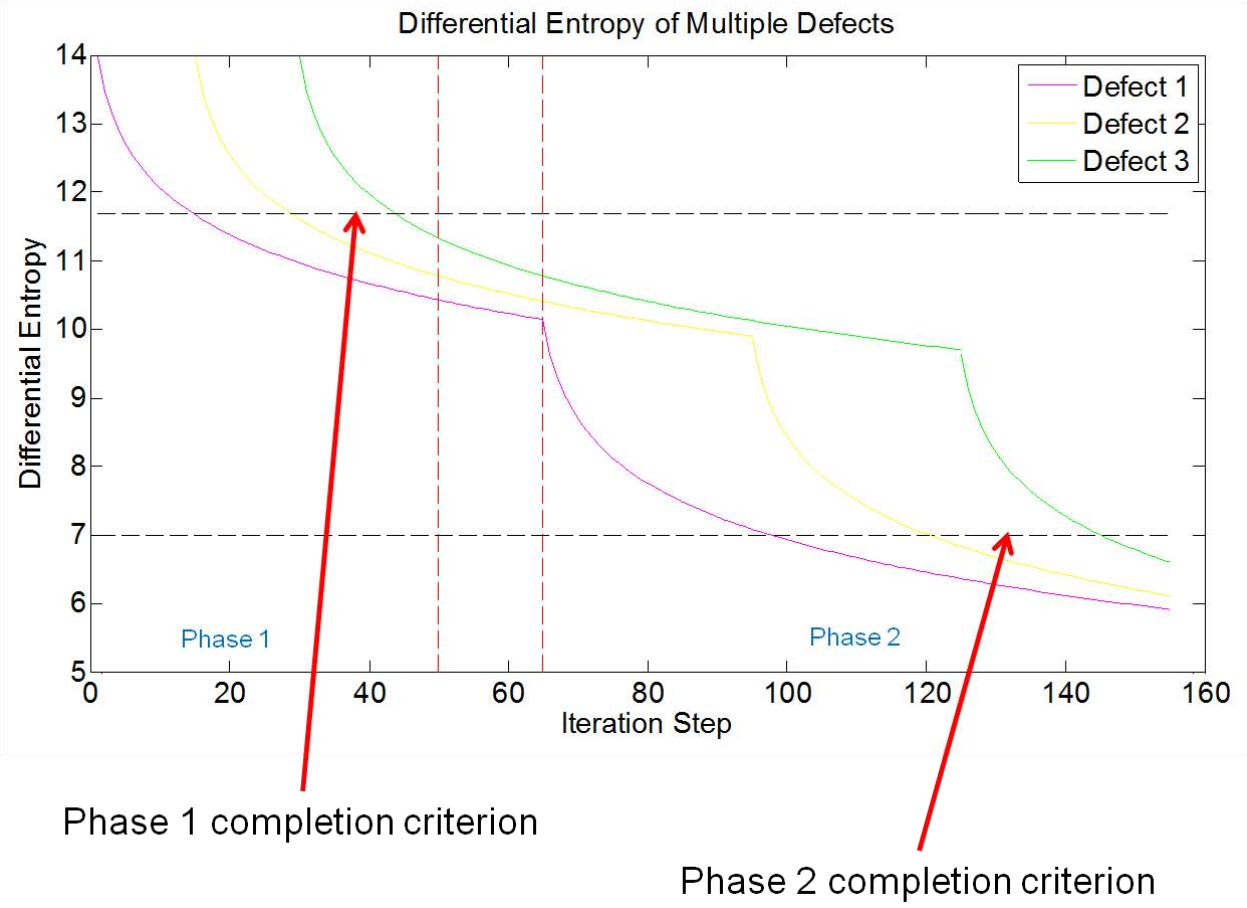

Conclusion

The system constructed from this project has the following capabilities:

- Automated techniques to characterize defects;
- Technique that stochastically estimates the states of defects;
- Technique that allows active sensing;
- Technique that enhances current signal analysis;

Acknowledgement

The investigators would like to primarily express their sincere gratitude to Drs. Kumar Jata and Ken Goretta at AOARD and Drs. Victor G. at University of South Carolina and David Stargel at AFOSR for their support in this project. The appreciation also goes to Dr. John G. Michopulos at NRL and Drs. Jinquan Cheng and Lin Chi Mak at Virginia Tech.

Publications

1. Furukawa and Pan, "Stochastic Estimation of Elastic Constants for Anisotropic Materials, International Journal for Numerical Methods in Engineering, Vol. 81, pp. 429-452, 2010.
2. Pan, Cheng and Furukawa, "Energy-based Characterization based on Multi-sensor Data Fusion", Key Engineering Materials Journal, in print.
3. Jan Wei Pan, Jinquan Cheng and Tomonari Furukawa, "Multi-sensor Data Fusion for Stochastic Energy-based Characterization", International Journal of Computational Methods, in print.
4. Furukawa, Michopoulos and Pan, "Generalized Recursive Technique for Energy-based Characterization," International Journal for Numerical Methods in Engineering, in print.
5. Pan, Furukawa, Man, Iliopoulos, Michopoulos, Hermanson, "An Energy-based Computational and Experimental Method for the Elastic Characterization of Materials," Acta Mechanica Solida Sinica, submitted.
6. Lim and Furukawa, "Calibration-free Image Sensor Model for an Arbitrary Pan-Tilt Plane of View," International Journal of Automation and Control, accepted.
7. Furukawa, Lim and Michopoulos, "Identification of Defects under Sensor Uncertainties," International Journal for Numerical Methods in Engineering, submitted.
8. Lim, Furukawa and Xu, "Construction of Observation Likelihoods for Stochastic Defect Identification," International Journal for Numerical Methods in Engineering, submitted.
9. Lim, Furukawa, Cheng and Michopoulos, "Experimental Validation of Belief Driven Rapid Field Inspection," Experimental Mechanics, in preparation.